Hsp90 and HSF-1 was not altered after 17-AAG treatment, coimmunoprecipitation of HSF-1 with Hsp90 in the spinal cord and skeletal muscle was significantly reduced ($P < 0.01$ for both) after 17-AAG treatment (**Supplementary Fig. 4** online), indicating that this drug induces Hsps through activation of HSF-1.

DISCUSSION

Our study showed that the polyQ-expanded mutant AR present in SBMA was preferentially degraded by treatment with 17-AAG. Elimination of mutant AR was mediated through its preferential incorporation into the Hsp90-chaperone complex, where it is then prone to proteasomal degradation. Owing to this mechanism, 17-AAG markedly ameliorated motor phenotypes of the SBMA mouse model without toxicity. Our present data from the mouse model also confirmed that 17-AAG passes through the blood-brain barrier as previously reported[42], and that it reaches a concentration high enough to have effects in the central nervous system.

Recently, some antitumor agents have been therapeutically applied to neurodegenerative diseases[43,44]. Most antitumor agents have some cytotoxic effects on normal cells, which must be overcome in any clinical application against neurodegeneration. Because neurodegenerative diseases generally follow a chronic progression and the medical treatment is, thus, long-standing compared to that for malignancy, the toxic side effects should be extensively suppressed. In contrast to general antitumor agents, the effects of 17-AAG have been known to have a high selectivity for tumor cells. This selectivity results from the high affinity of 17-AAG for the Hsp90 client oncoproteins when they are incorporated in the Hsp90-dependent multichaperone complex, thereby increasing their binding affinity for 17-AAG more than 100-fold[19]. This high selectivity of 17-AAG for the incorporated Hsp90 client protein eventually minimizes its toxic side effects and renders it very feasible for clinical applications, especially for neurodegenerative diseases. In fact, our transgenic mice were free from obvious side effects after the consecutive administration of 17-AAG for 20 weeks.

The major pharmacological effect of 17-AAG is to promote the dissociation of p23 from Hsp90 client protein complexes[10–12,16]. In this study, we showed that the mutant AR with an expanded polyQ had a higher association with p23 than did the wild-type AR. We consider this significantly higher association between the mutant AR and p23, particularly compared with the wild-type AR, to be the essential basis for preferential degradation of the polyQ-expanded mutant AR after 17-AAG treatment. Furthermore, the increase in Hop and decrease in p23 in the mutant AR-bound Hsp90 complex after 17-AAG treatment strongly supports the view that Hsp90 complexes were shifted to the proteasome-targeting form by 17-AAG, leading to proteasomal degradation of mutant AR. Given that the increase in Hop proteins in Hsp90 complexes and the decrease in p23 were only detected after the higher concentration of 17-AAG and after a very short period of incubation, this chaperone complex shift seems to be very rapid, as has been suggested previously[12].

Hsps, particularly Hsp70, have been shown to suppress aggregate formation and cellular toxicity in a wide range of polyQ disease models[21,36,45,46]. Geldanamycin has been considered a neuroprotective agent because of its ability to induce Hsp70 (refs. 22–24,27), and in polyQ diseases, has been proven to suppress aggregation of mutant huntingtin protein in a cultured-cell model through the induction of Hsp70 and Hsp40 (refs. 22,23). Hsp90 inhibitors have also been shown to be effective in animal models of Parkinson disease[24], stroke[27] and autoimmune encephalomyelitis[28]. It was thought that these effects were based only on the ability of the Hsp90 inhibitors to induce Hsps. As shown in this study, however, 17-AAG induced only limited amounts of Hsp70 and Hsp40 *in vivo*. Furthermore, our results suggest that the pathway for mutant AR degradation by 17-AAG through the Hsp90-client protein complex system is predominant. 17-AAG is expected to exert the most effective therapeutic potential for diseases in which the disease-causing protein belongs to the Hsp90 client protein family.

Mutant p53, which is present in nearly half of all malignancies and is an Hsp90 client protein, shows a much higher sensitivity to Hsp90 inhibitors than does wild-type p53 (ref. 47), just as AR, in its polyQ-expanded mutant form, acquired higher sensitivity to the Hsp90 inhibitor. In the case of neurodegenerative diseases, phosphorylated tau would be one of the target proteins of Hsp90 inhibitors, because geldanamycin substantially reduces the total amount of phosphorylated tau[25,26], and also inhibits tau aggregation[25]. According to these previous reports, our data suggest that 17-AAG would also be a candidate for a therapeutic approach to a wide range of tauopathies. The successful application of 17-AAG to polyQ diseases other than SBMA remains to be seen. But, as a previous report showed, the blockage of pathogenetic gene expression could reversibly reduce nuclear inclusions and reactive gliosis in a mouse model of Huntington disease by self-cleaning functions[48]. Indeed, one therapeutic approach, which directly reduced abnormal protein using RNA interference, proved to be beneficial in a mouse model of SCA1 (ref. 49). There is no doubt that the reduction of disease-causing protein would be beneficial in polyQ diseases. Therefore, once it is proven that the disease-causing proteins belong to the Hsp90 client protein family and have high affinities to Hsp90 inhibitors, 17-AAG is expected to preferentially degrade the expanded polyQ-containing disease proteins and, thus, would be a good candidate for clinical therapeutics.

In conclusion, we have shown the efficacy and safety of 17-AAG in a model mouse of SBMA, a neurodegenerative disease, and considerably extended the therapeutic application of 17-AAG beyond oncological diseases. In addition, we have documented the differential degradation efficacy of a polyQ-expanded mutant protein compared with its wild-type form. This strategy is apparently different from the previous strategy for polyQ diseases, which unavoidably allowed abnormal protein to remain and placed much value mainly on the inhibition of protein aggregation. 17-AAG, directly reducing disease-causing protein itself, presents a new therapeutic avenue for SBMA, and has potentially widespread application for other neurodegenerative diseases.

METHODS

DNA transfection. We constructed full-length ARs by subcloning AR inserts derived from pSP64-AR24 or pSP64-AR97 (ref. 46) into the pCR3.1 mammalian expression vector (Invitrogen). We plated SH-SY5Y cells in 6-cm dishes and transfected each dish with 8 μg of the vector containing AR24 or AR97 using Lipofectamine 2000 (Invitrogen) according to the manufacturer's instructions. We cultured the cells for 48 h. In this culture system, we detected a band of monomeric mutant AR in the separating gel, but could hardly detect the high molecular–weight mutant AR protein complex, which was retained in the stacking gel.

Neurological and behavioral assessment of SBMA model mice. We generated and maintained the AR-24Q and AR-97Q mice as previously described[35] (**Supplementary Methods** online). All animal experiments were performed in accordance with the National Institutes of Health Guide for the Care and Use of Laboratory Animals and under the approval of the Nagoya University Animal Experiment Committee. We performed the mouse rotarod task and cage activity as described previously[35]. The investigators in the behavioral assessment were blinded to the treatments.

Therapeutic agents and protocol for administration. We obtained 17-AAG, also known as NSC 330507, from the Regulatory Affairs Branch, Division of

Cancer Treatment and Diagnosis, National Cancer Institute and Kosan Biosciences. For cultured-cell models, we diluted a 1.8 mM stock solution of 17-AAG in DMSO into fresh medium to give final concentrations of 18–360 nM. In the cycloheximide study, we treated cells for 48 h with 17-AAG in the presence of 5 μg/ml cycloheximide (Sigma). To show pharmacological changes in the AR-Hsp90 complex, we exposed cultured cells for 30 min to 17-AAG at concentrations of 0.36, 3.6 and 36 μM 48 h after transfection. In the proteasome-inhibitory study, we exposed cultured cells for 6 h to 36 μM 17-AAG, and 5, 10 and 20 μM MG132 (Sigma) beginning 48 h after transfection.

For mouse models, we stored 50 mg/ml stock solutions of 17-AAG dissolved in DMSO at –20 °C. We began 17-AAG treatments when mice attained the age of 5 weeks, and continued them until mice were 25 weeks old. Normal male littermates, AR-24Q mice and AR-97Q mice received 50 μl intraperitoneal injections of 2.5 or 25 mg/kg 17-AAG three times a week on alternate days; control mice received DMSO alone.

Protein expression analysis. We lysed cells in CelLytic-M Mammalian Cell Lysis/Extraction Reagent (Sigma) and centrifuged them at 15,000*g* for 15 min at 4 °C. We homogenized the tissues from 16-week-old mice in CelLytic-M (Sigma) and centrifuged them at 2,500*g* for 15 min at 4 °C. Primary antibodies were as follows: AR-specific antibody (N-20 or H280; Santa Cruz); Hsp70-specific antibody (SPA-810; Stressgen); Hsp40-specific antibody (SPA-400; Stressgen); Hsp90-specific antibody (SPA-835; Stressgen); Hop-specific antibody (SRA-1500; Stressgen); p23-specific antibody (MA3-414; Affinity BioReagents); HSF-1–specific antibody (SPA-901; Stressgen); p85-specific antibody (Upstate); and α-tubulin–specific antibody (T9026; Sigma). We used the LAS-3000 imaging system to produce digital images and to quantify band intensities, which we then analyzed with Image Gauge software version 4.22 (Fujifilm). Densitometric values of AR, Hsp70, Hsp40 and Hsp90 were normalized to those of endogenous p85 or α-tubulin. Relative signal intensity (R.S.I.) was computed as the signal intensity of each sample divided by that of DMSO-treated cells or DMSO-treated mice.

We performed immunoprecipitation from cultured cells using 300 μg total protein lysate from cells, 10 μl Protein G Sepharose (Amersham) and 5 μl AR-specific antibody (N-20). For experiments involving coprecipitation of AR, we lysed cells in molybdate-containing lysis buffer[11,12,16]. Immunoprecipitation from mouse tissues was performed using 1 mg total protein lysed in CelLytic-M (Sigma). R.S.I. was computed as the signal intensity of each sample divided by that of AR-24Q cells, DMSO-treated cells or DMSO-treated mice.

Pulse-chase labeling assay. We transfected cells as described above, starved them for 1 h, and then labeled them for 1 h with 150 μCi of Redivue Pro-Mix L-[35S] *in vitro* cell-labeling mix (Amersham) per milliliter. We chased the cells for the indicated time intervals in complete medium with DMSO or 360 nM 17-AAG. We performed immunoprecipitation using equivalent amounts of protein lysates as described above, and analyzed by phosphorimaging (Typhoon 8600 phosphorimager; Amersham) and Image Gauge software, version 4.22 (Fujifilm).

Quantitative real-time RT-PCR. We determined the levels of AR mRNA by real-time Taqman PCR by the iCycler system (Bio-Rad) as previously described[50]. R.S.I. was computed as the signal intensity of each sample divided by that of DMSO-treated cells or DMSO-treated control mice.

Immunohistochemistry and histopathology. We prepared tissues as previously described[35–38]. We incubated the tissue sections with expanded polyQ-specific antibody (1:10,000, 1C2; Chemicon) and GFAP-specific antibody (1:1,000, Boehringer Manheim). We air-dried 6 μm–thick paraffin-embedded sections of the gastrocnemius muscles and stained them with hematoxylin and eosin. For quantification of 1C2-positive cells, we counted the number of 1C2-positive cells of the thoracic spinal cord and gastrocnemius muscle in each individual mouse as previously described[36].

Statistical analysis. We analyzed data by unpaired *t*-tests and Kaplan-Meier and log-rank tests for survival rate using Statview software version 5 (HULINKS). We examined statistical significance of the drug-dose dependency by the Williams test for multiple comparisons using Microsoft Excel 2004 (Microsoft).

Accession codes. BIND identifiers (http://bind.ca): 316918.

Note: Supplementary information is available on the Nature Medicine website.

ACKNOWLEDGMENTS

We thank National Cancer Institute and Kosan Biosciences for kindly providing 17-AAG. This work was supported by a Center of Excellence (COE) grant from the Ministry of Education, Culture, Sports, Science and Technology, Japan, and by grants from the Ministry of Health, Labor and Welfare, Japan.

COMPETING INTERESTS STATEMENT

The authors declare that they have no competing financial interests.

Published online at http://www.nature.com/naturemedicine/
Reprints and permissions information is available online at http://npg.nature.com/reprintsandpermissions/

1. Pratt, W.B. & Toft, D.O. Regulation of signaling protein function and trafficking by the hsp90/hsp70-based chaperone machinery. *Exp. Biol. Med. (Maywood)* **228**, 111–133 (2003).
2. Neckers, L., Schulte, T.W. & Mimnaugh, E. Geldanamycin as a potential anti-cancer agent: its molecular target and biochemical activity. *Invest. New Drugs* **17**, 361–373 (1999).
3. Supko, J.G., Hickman, R.L., Grever, M.R. & Malspeis, L. Preclinical pharmacologic evaluation of geldanamycin as an antitumor agent. *Cancer Chemother. Pharmacol.* **36**, 305–315 (1995).
4. Schulte, T.W. & Neckers, L.M. The benzoquinone ansamycin 17-allylamino-17-demethoxygeldanamycin binds to HSP90 and shares important biologic activities with geldanamycin. *Cancer Chemother. Pharmacol.* **42**, 273–279 (1998).
5. Page, J. *et al.* Comparison of geldanamycin (NSC-122750) and 17-allylaminogeldanamycin (NSC-330507D) toxicity in rats. *Proc. Am. Assoc. Cancer Res.* **38**, 308 (1997).
6. Sullivan, W. *et al.* Nucleotides and two functional states of hsp90. *J. Biol. Chem.* **272**, 8007–8012 (1997).
7. Bagatell, R. *et al.* Destabilization of steroid receptors by heat shock protein 90-binding drugs: a ligand-independent approach to hormonal therapy of breast cancer. *Clin. Cancer Res.* **7**, 2076–2084 (2001).
8. Neckers, L. Heat shock protein 90 inhibition by 17-allylamino-17-demethoxygeldanamycin: a novel therapeutic approach for treating hormone-refractory prostate cancer. *Clin. Cancer Res.* **8**, 962–966 (2002).
9. Felts, S.J. & Toft, D.O. p23, a simple protein with complex activities. *Cell Stress Chaperones* **8**, 108–113 (2003).
10. Johnson, J.L. & Toft, D.O. Binding of p23 and hsp90 during assembly with the progesterone receptor. *Mol. Endocrinol.* **9**, 670–678 (1995).
11. Smith, D.F. *et al.* Progesterone receptor structure and function altered by geldanamycin, an hsp90-binding agent. *Mol. Cell. Biol.* **15**, 6804–6812 (1995).
12. Whitesell, L. & Cook, P. Stable and specific binding of heat shock protein 90 by geldanamycin disrupts glucocorticoid receptor function in intact cells. *Mol. Endocrinol.* **10**, 705–712 (1996).
13. Schneider, C. *et al.* Pharmacologic shifting of a balance between protein refolding and degradation mediated by Hsp90. *Proc. Natl. Acad. Sci. USA* **93**, 14536–14541 (1996).
14. Solit, D.B. *et al.* 17-Allylamino-17-demethoxygeldanamycin induces the degradation of androgen receptor and HER-2/neu and inhibits the growth of prostate cancer xenografts. *Clin. Cancer Res.* **8**, 986–993 (2002).
15. Vanaja, D.K., Mitchell, S.H., Toft, D.O. & Young, C.Y. Effect of geldanamycin on androgen receptor function and stability. *Cell Stress Chaperones* **7**, 55–64 (2002).
16. Beliakoff, J. *et al.* Hormone-refractory breast cancer remains sensitive to the antitumor activity of heat shock protein 90 inhibitors. *Clin. Cancer Res.* **9**, 4961–4971 (2003).
17. Bonvini, P., Dalla Rosa, H., Vignes, N. & Rosolen, A. Ubiquitination and proteasomal degradation of nucleophosmin-anaplastic lymphoma kinase induced by 17-allylamino-demethoxygeldanamycin: role of the co-chaperone carboxyl heat shock protein 70-interacting protein. *Cancer Res.* **64**, 3256–3264 (2004).
18. Mimnaugh, E.G., Chavany, C. & Neckers, L. Polyubiquitination and proteasomal degradation of the p185c-erbB-2 receptor protein-tyrosine kinase induced by geldanamycin. *J. Biol. Chem.* **271**, 22796–22801 (1996).
19. Kamal, A. *et al.* A high-affinity conformation of Hsp90 confers tumour selectivity on Hsp90 inhibitors. *Nature* **425**, 407–410 (2003).
20. Whitesell, L., Bagatell, R. & Falsey, R. The stress response: implications for the clinical development of hsp90 inhibitors. *Curr. Cancer Drug Targets* **3**, 349–358 (2003).
21. Muchowski, P.J. & Wacker, J.L. Modulation of neurodegeneration by molecular chaperones. *Nat. Rev. Neurosci.* **6**, 11–22 (2005).
22. Sittler, A. *et al.* Geldanamycin activates a heat shock response and inhibits huntingtin aggregation in a cell culture model of Huntington's disease. *Hum. Mol. Genet.* **10**, 1307–1315 (2001).
23. Hay, D.G. *et al.* Progressive decrease in chaperone protein levels in a mouse model of Huntington's disease and induction of stress proteins as a therapeutic approach. *Hum. Mol. Genet.* **13**, 1389–1405 (2004).
24. Auluck, P.K. & Bonini, N.M. Pharmacological prevention of Parkinson disease in *Drosophila*. *Nat. Med.* **8**, 1185–1186 (2002).
25. Dou, F. *et al.* Chaperones increase association of tau protein with microtubules. *Proc. Natl. Acad. Sci. USA* **100**, 721–726 (2003).

26. Petrucelli, L. *et al.* CHIP and Hsp70 regulate tau ubiquitination, degradation and aggregation. *Hum. Mol. Genet.* **13**, 703–714 (2004).
27. Lu, A., Ran, R., Parmentier-Batteur, S., Nee, A. & Sharp, F.R. Geldanamycin induces heat shock proteins in brain and protects against focal cerebral ischemia. *J. Neurochem.* **81**, 355–364 (2002).
28. Murphy, P. *et al.* Suppressive effects of ansamycins on inducible nitric oxide synthase expression and the development of experimental autoimmune encephalomyelitis. *J. Neurosci. Res.* **67**, 461–470 (2002).
29. La Spada, A.R., Wilson, E.M., Lubahn, D.B., Harding, A.E. & Fischbeck, K.H. Androgen receptor gene mutations in X-linked spinal and bulbar muscular atrophy. *Nature* **352**, 77–79 (1991).
30. Sobue, G. *et al.* X-linked recessive bulbospinal neuronopathy. A clinicopathological study. *Brain* **112**, 209–232 (1989).
31. Zoghbi, H.Y. & Orr, H.T. Glutamine repeats and neurodegeneration. *Annu. Rev. Neurosci.* **23**, 217–247 (2000).
32. Tanaka, F. *et al.* Founder effect in spinal and bulbar muscular atrophy (SBMA). *Hum. Mol. Genet.* **5**, 1253–1257 (1996).
33. Doyu, M. *et al.* Severity of X-linked recessive bulbospinal neuronopathy correlates with size of the tandem CAG repeat in androgen receptor gene. *Ann. Neurol.* **32**, 707–710 (1992).
34. Adachi, H. *et al.* Widespread nuclear and cytoplasmic accumulation of mutant androgen receptor in SBMA patients. *Brain* **128**, 659–670 (2005).
35. Katsuno, M. *et al.* Testosterone reduction prevents phenotypic expression in a transgenic mouse model of spinal and bulbar muscular atrophy. *Neuron* **35**, 843–854 (2002).
36. Adachi, H. *et al.* Heat shock protein 70 chaperone overexpression ameliorates phenotypes of the spinal and bulbar muscular atrophy transgenic mouse model by reducing nuclear-localized mutant androgen receptor protein. *J. Neurosci.* **23**, 2203–2211 (2003).
37. Katsuno, M. *et al.* Leuprorelin rescues polyglutamine-dependent phenotypes in a transgenic mouse model of spinal and bulbar muscular atrophy. *Nat. Med.* **9**, 768–773 (2003).
38. Minamiyama, M. *et al.* Sodium butyrate ameliorates phenotypic expression in a transgenic mouse model of spinal and bulbar muscular atrophy. *Hum. Mol. Genet.* **13**, 1183–1192 (2004).
39. Bailey, C.K., Andriola, I.F., Kampinga, H.H. & Merry, D.E. Molecular chaperones enhance the degradation of expanded polyglutamine repeat androgen receptor in a cellular model of spinal and bulbar muscular atrophy. *Hum. Mol. Genet.* **11**, 515–523 (2002).
40. Lieberman, A.P., Harmison, G., Strand, A.D., Olson, J.M. & Fischbeck, K.H. Altered transcriptional regulation in cells expressing the expanded polyglutamine androgen receptor. *Hum. Mol. Genet.* **11**, 1967–1976 (2002).
41. Zou, J., Guo, Y., Guettouche, T., Smith, D.F. & Voellmy, R. Repression of heat shock transcription factor HSF1 activation by HSP90 (HSP90 complex) that forms a stress-sensitive complex with HSF1. *Cell* **94**, 471–480 (1998).
42. Egorin, M.J. *et al.* Plasma pharmacokinetics and tissue distribution of 17-(allylamino)-17-demethoxygeldanamycin (NSC 330507) in CD2F1 mice1. *Cancer Chemother. Pharmacol.* **47**, 291–302 (2001).
43. Ravikumar, B. *et al.* Inhibition of mTOR induces autophagy and reduces toxicity of polyglutamine expansions in fly and mouse models of Huntington disease. *Nat. Genet.* **36**, 585–595 (2004).
44. Ferrante, R.J. *et al.* Chemotherapy for the brain: the antitumor antibiotic mithramycin prolongs survival in a mouse model of Huntington's disease. *J. Neurosci.* **24**, 10335–10342 (2004).
45. Cummings, C.J. *et al.* Chaperone suppression of aggregation and altered subcellular proteasome localization imply protein misfolding in SCA1. *Nat. Genet.* **19**, 148–154 (1998).
46. Kobayashi, Y. *et al.* Chaperones Hsp70 and Hsp40 suppress aggregate formation and apoptosis in cultured neuronal cells expressing truncated androgen receptor protein with expanded polyglutamine tract. *J. Biol. Chem.* **275**, 8772–8778 (2000).
47. Blagosklonny, M.V., Toretsky, J., Bohen, S. & Neckers, L. Mutant conformation of p53 translated *in vitro* or *in vivo* requires functional HSP90. *Proc. Natl. Acad. Sci. USA* **93**, 8379–8383 (1996).
48. Yamamoto, A., Lucas, J.J. & Hen, R. Reversal of neuropathology and motor dysfunction in a conditional model of Huntington's disease. *Cell* **101**, 57–66 (2000).
49. Xia, H. *et al.* RNAi suppresses polyglutamine-induced neurodegeneration in a model of spinocerebellar ataxia. *Nat. Med.* **10**, 816–820 (2004).
50. Ishigaki, S. *et al.* X-Linked inhibitor of apoptosis protein is involved in mutant SOD1-mediated neuronal degeneration. *J. Neurochem.* **82**, 576–584 (2002).

Developmental Cell, Vol. 9, 389–402, September, 2005, Copyright ©2005 by Elsevier Inc. DOI 10.1016/j.devcel.2005.08.001

Akt/PKB Regulates Actin Organization and Cell Motility via Girdin/APE

Atsushi Enomoto,[1] Hideki Murakami,[1] Naoya Asai,[1] Nobuhiro Morone,[2,5] Takashi Watanabe,[3] Kumi Kawai,[4] Yoshiki Murakumo,[1] Jiro Usukura,[2] Kozo Kaibuchi,[3] and Masahide Takahashi[1,4,*]

[1]Department of Pathology
[2]Department of Cell Biology and Anatomy
[3]Department of Cell Pharmacology
[4]Division of Molecular Pathology
Center for Neurological Disease and Cancer
Nagoya University Graduate School of Medicine
65 Tsurumai-cho
Showa-ku, Nagoya
Aichi 466-8550
Japan
[5]Department of Ultrastructural Research
National Institute of Neuroscience
National Center of Neurology and Psychiatry
Kodaira
Tokyo 187-8502
Japan

Summary

The serine/threonine kinase Akt (also called protein kinase B) is well known as an important regulator of cell survival and growth and has also been shown to be required for cell migration in different organisms. However, the mechanism by which Akt functions to promote cell migration is not understood. Here, we identify an Akt substrate, designated Girdin/APE (Akt-phosphorylation enhancer), which is an actin binding protein. Girdin expresses ubiquitously and plays a crucial role in the formation of stress fibers and lamellipodia. Akt phosphorylates serine at position 1416 in Girdin, and phosphorylated Girdin accumulates at the leading edge of migrating cells. Cells expressing mutant Girdin, in which serine 1416 was replaced with alanine, formed abnormal elongated shapes and exhibited limited migration and lamellipodia formation. These findings suggest that Girdin is essential for the integrity of the actin cytoskeleton and cell migration and provide a direct link between Akt and cell motility.

Introduction

In multicellular organisms, cell migration is a highly integrated process that orchestrates embryonic morphogenesis, contributes to tissue repair and regeneration, and drives disease progression in cancer, atherosclerosis, and immune diseases (Lauffenburger and Horwitz, 1996; Ridley et al., 2003). Cell migration that is initiated in response to multiple extracellular cues such as growth factors and cell-extracellular matrix adhesions requires dynamic and spatially regulated changes of the actin cytoskeleton, microtubules, adhesion molecules, and extracellular matrix. This function is mediated and coordinated by many different intracellular signaling molecules, including the Rho family of small GTPases, Ca^{2+}-regulated proteins, mitogen-activated protein kinases (MAPKs), protein kinase C, phosphatidylinositide kinases, and tyrosine kinases (Etienne-Manneville and Hall, 2002; Ridley, 2001).

Akt, also known as protein kinase B (PKB), is a serine/threonine kinase activated downstream of class I phosphatidylinositol 3-kinase (PI3K) and various receptors. It has emerged as the key regulator for many signal transduction pathways, modulating multiple processes such as cell survival, proliferation, growth, angiogenesis, and glucose metabolism (Brazil et al., 2002; Datta et al., 1999; Vivanco and Sawyers, 2002). Akt substrates include transcription factors, antiapoptotic proteins, and protein kinases that regulate protein synthesis. In addition, Akt has also been shown to be required for chemotaxis in mammalian leukocytes and *Dictyostelium* cells (Chung et al., 2001; Meili et al., 1999; Merlot and Firtel, 2003). A growing body of evidence indicates that Akt promotes cell motility in mammalian fibroblasts and tumor cells (Higuchi et al., 2001; Kim et al., 2001; Morales-Ruiz et al., 2000). PI3K and the tumor suppressor protein PTEN, upstream regulators of Akt activity, have been shown to be essential for cell migration and the establishment of cell polarity (Merlot and Firtel, 2003). Moreover, clinical studies have revealed that cancer patients whose tumors have increased Akt expression tend to have more invasive and metastatic diseases, which are associated with a poor prognosis (Scheid and Woodgett, 2001; Vivanco and Sawyers, 2002). These findings indicate that Akt is involved in cell migration and invasion in cells of many different organisms. However, the molecular mechanisms of how Akt regulates the cytoskeleton and thereby modulates cell motility are largely unknown. The localization of the pleckstrin-homology (PH) domain of Akt at the leading edge during chemotaxis in neutrophils (Servant et al., 2000), *Dictyostelium* cells (Meili et al., 1999), and mammalian fibroblasts (Higuchi et al., 2001) suggests that this kinase phosphorylates and regulates yet to be identified proteins that are involved in remodeling of the leading edge (Merlot and Firtel, 2003).

In eukaryotic cells, the integrity and dynamic reorganization of the actin cytoskeleton are essential for cellular morphogenesis and generation of the forces needed for motility. Actin bundles provide tensile strength, whereas the crosslinked three-dimensional orthogonal networks provide elasticity (Stossel et al., 2001). At the leading edge, migrating cells create short-branched actin networks in order to sustain a pushing force (Pollard and Borisy, 2003). These features of the actin cytoskeleton are regulated by multiple actin filament crosslinking/bundling proteins that include the fimbrin/α-actinin/filamin (also termed ABP-280), villin, scruin, and fascin families (Pollard, 2002; Revenu et al., 2004). Although each actin crosslinking protein has a distinct function that is essential for normal physiology, appar-

*Correspondence: mtakaha@med.nagoya-u.ac.jp

ent redundancy of these proteins has been suggested (Pollard, 2002). Organisms or cells that lack some actin crosslinking proteins still survive despite large defects in cell behavior and growth rate. *Dictyostelium* cells that lacked α-actinin showed no motility defects, with deficiencies only in behavior and architecture (Pollard, 2002; Rivero et al., 1996; Stossel et al., 2001). A cell line established from human malignant melanoma, which expressed no filamin, could not undergo locomotion in response to growth factors but was still able to survive (Stossel et al., 2001). These findings suggest that these crosslinking proteins share overlapping functions in the actin system, and that the inventory of important actin crosslinking proteins may still be incomplete (Pollard, 2002).

In this study, we identified a novel, to our knowledge, substrate of Akt. We designate it Girdin (girders of actin filaments), because RNA interference (RNAi)-mediated depletion of Girdin gives rise to the disruption of stress fibers and limited extension of lamellipodia in fibroblasts. A recently published paper also identified the same protein designated APE (Akt-phosphorylation enhancer) as an Akt binding protein (Anai et al., 2005), although a role in actin organization was not characterized. We show that the phosphorylation of Girdin/APE by Akt occurs at the leading edge of migrating cells, which controls the association between Girdin and the plasma membrane and subsequently facilitates the formation of lamellipodium.

Results

Identification of an Akt-Interacting Protein, Girdin/APE

To identify novel Akt substrates, we performed a yeast two-hybrid screen with full-length human Akt1 as bait and searched for interacting proteins by using a human fetal brain cDNA library. Two independent and overlapping clones (F-10 and F-12) encoding a novel gene product were identified. When expressed in yeast, the protein encoded by the F-10 and F-12 cDNAs was shown to interact only with the carboxyl-terminal regulatory domain (RD) of Akt1 (Figures 1A and 1B). Use of 5′-rapid amplification of cDNA ends (5′-RACE) provided a clone comprising the entire coding region with an additional 3.8 kb cDNA of contiguous 5′ sequence. The full-length cDNA included an open reading frame of 5610 base pairs (bp) and was predicted to encode a novel, to our knowledge, protein of 1870 amino acids, which we designated Girdin, with a calculated molecular mass of 220 kilodaltons (kDa) (Figure S1; see the Supplemental Data available with this article online). Database searches revealed homologs in mouse, rat, and *Drosophila* (not shown), but no apparent matches in *Caenorhabditis elegans* and *Dictyostelium*. A mouse ortholog of Girdin named APE was recently reported (Anai et al., 2005).

The structure of Girdin predicted by the COILS algorithm (Lupas et al., 1991) showed a tendency to assume an α-helical coiled-coil conformation in its middle domain, between Ala-253 and Lys-1375, with a high coiled-coil probability of 1.0 (Figure 1C). The predicted coiled-coil domain contains 135 continuous heptad repeats ($[abcdefg]_{135}$) that are typical of α-helical coiled-coils (Figure S1). The 9.5 kb Girdin transcript was found to be expressed ubiquitously in various human tissues by high-stringency Northern blot analysis (Figure 1D). To facilitate further studies on Girdin, we generated a polyclonal antibody (Ab) raised against its 19 C-terminal amino acids. Western blot analysis revealed that the anti-Girdin Ab recognizes a specific band of relative molecular mass of 250 kDa in human brain and testis lysates (Figure 1E).

Because of the existence of an α-helical coiled-coil domain in the primary structure of Girdin, we investigated the possibility of Girdin being an oligomeric molecule. Cell lysates from COS7 cells were analyzed by Western blot analysis with anti-Girdin Ab, either directly or after crosslinking with 100 μM Bis(sulfosuccinimidyl) suberate (BS^3) (Figure 1F). In the presence of BS^3, Girdin was predominantly found in a complex of large molecular mass. To determine the molecular mass of Girdin-containing protein complexes in intact cells, we subjected the lysates from COS7 cells to gel filtration (Figure S2). The data confirmed that Girdin forms a large protein complex. We next tested whether the NT and CT domains contribute to the oligomerization of Girdin. When V5 epitope-tagged NT (NT-V5) and myc epitope-tagged NT (NT-myc) were expressed in COS7 cells, a complex of these two NT domains was observed (Figure 1G). This result implies that the NT domain facilitates the oligomerization of Girdin. In contrast, the CT domain did not form an oligomer in cells (data not shown). Analysis of the lysates from COS7 cells expressing the NT domain by gel filtration suggested that the NT domain forms a dimer (Figure S2).

Akt Phosphorylates Girdin In Vitro and In Vivo

We initially used in vitro and in vivo assays to ascertain if Girdin and Akt physically interact with each other. Neither in vitro binding nor immunoprecipitation assays with various fragments of Girdin and Akt demonstrated the formation of a stable complex of the two proteins (data not shown), suggesting that they may normally associate in a very transient manner, as observed for the interactions between protein kinases and their substrates (Brazil et al., 2002). Although Anai et al. (2005) observed a weak association of the two proteins by immunoprecipitation, the difference may be due to the experimental conditions used.

It has been established that Akt preferentially phosphorylates substrates that contain the sequence R-x-R-x-x-S/T (Alessi et al., 1996). The amino acid sequence adjacent to a serine at position 1416 (Ser-1416 indicated by the underlined "S," RERQKS) in the CT domain of Girdin conforms to this consensus sequence (Figure 2Aa). This is the only consensus site in the protein. Since the CT domain with the putative phosphorylation site is conserved in different mammalian Girdin homologs (data not shown), we asked whether Akt phosphorylates Girdin. An in vitro kinase assay revealed that Girdin CT wild-type (WT), but not its Ser → Ala mutant (SA), was phosphorylated by active Akt, indicating that Akt directly phosphorylates the Ser-1416 in vitro (Figure 2Ab). In contrast, neither the NT nor the coiled-coil domain of Girdin was phosphorylated by Akt in vitro (Figure 2B).

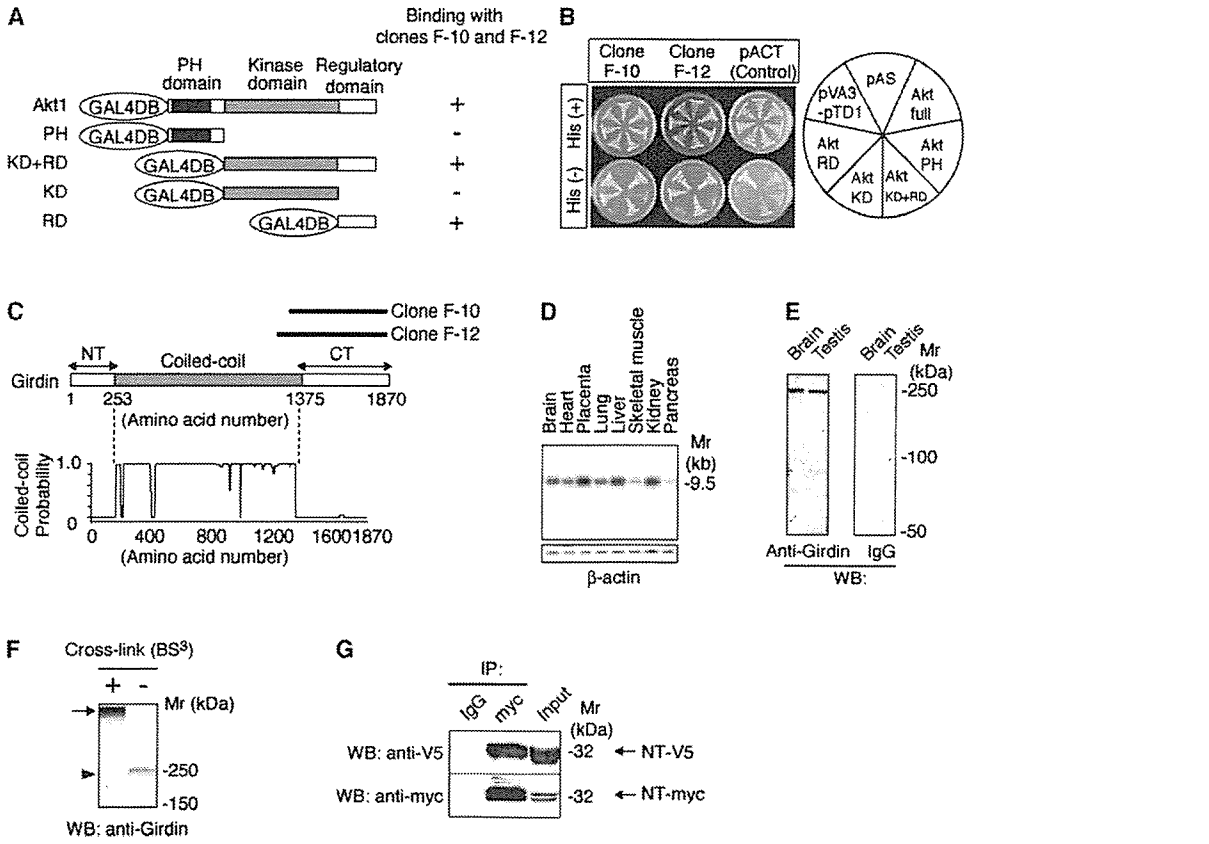

Figure 1. Identification, Primary Structure, and Expression of Girdin

(A) Schematic illustration of bait constructs for yeast two-hybrid binding assays. The cDNA fragments corresponding to the indicated domains of human Akt1 were fused in frame to the DNA binding domain of GAL4 transcription factor (GAL4DB) in the pAS2 vector. PH, pleckstrin homology domain; KD, catalytic kinase domain; RD, regulatory domain.

(B) Interactions of clones F-10 and F-12 with human Akt1 in yeast two-hybrid binding assays. pAS, a negative control; pVA3-pTD1, a positive control; His, histidine.

(C) Schematic presentation of Girdin and structure predictions provided by the COILS algorithm.

(D) Ubiquitous expression of Girdin mRNA in human adult tissues. A human multiple-tissue Northern (MTN) blot (Clontech) was hybridized with a probe corresponding to the 3′ region of Girdin cDNA.

(E) Endogenous Girdin in lysates from human brain and testis was detected with anti-Girdin polyclonal antibody, but not with rabbit IgG, under reducing conditions.

(F) Detection of a large complex formation by endogenous Girdin. COS7 postnuclear supernatants were subjected to Western blot analysis by using anti-Girdin antibody, either directly (–) or after crosslinking with 100 μM BS^3 (+). The size of a band detected after crosslinking (arrow) is extremely large compared with that without crosslinking (arrowhead).

(G) The NT domain of Girdin forms an oligomer. NT-V5 and NT-myc were transfected into COS7 cells and immunoprecipitated with anti-myc antibody. NT-V5 was coimmunoprecipitated with NT-myc. The multiple bands in the lower panel may represent the degradation of NT-myc in cells.

In order to confirm that Ser-1416 is the site of Akt-catalyzed phosphorylation in vivo, we raised an antibody to a peptide that includes phosphorylated Ser-1416 and used it for Western blotting (Figure 2C). The anti-phospho Ser-1416 peptide antibody (anti-P-Girdin Ab) recognized the Girdin CT (WT) that was coexpressed with wild-type (Akt WT) or constitutively active Akt (Akt CA), but not with dominant-negative Akt (Akt DN). The anti-P-Girdin Ab did not recognize the Girdin CT (SA) mutant coexpressed with the Akt CA. These findings indicate that the anti-P-Girdin Ab specifically recognizes the Girdin CT phosphorylated at Ser-1416.

We next asked whether the anti-P-Girdin Ab can detect the endogenous Girdin phosphorylated in response to external stimuli that physiologically activate endogenous Akt. As shown in Figure 2D, the addition of epidermal growth factor (EGF) induced the phosphorylation of a protein that corresponds to immunoprecipitated Girdin (250 kDa) with a time course similar to that of Akt activation. In addition, the phosphorylation of Girdin was inhibited when cells were treated with the PI3K inhibitors LY294002 and Wortmannin, but not with the mitogen-activated protein kinase kinase 1 (MEK1) inhibitor PD98059. We therefore concluded that the phosphorylation of Girdin is induced by EGF in a PI3K-dependent manner. The expression of Akt WT and Akt CA, but not Akt DN, induced significant phosphorylation of Girdin (Figure 2E), indicating that active Akt alone is sufficient to induce its phosphorylation in cells. Moreover, Girdin phosphorylation was undetectable in

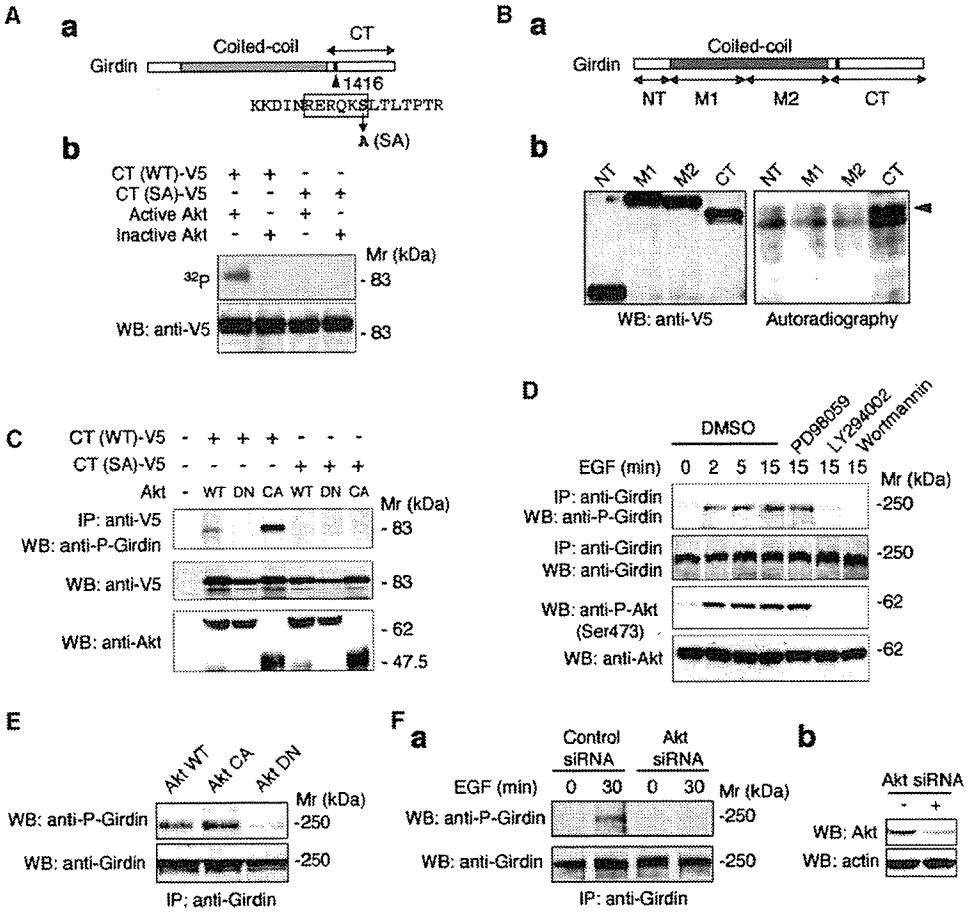

Figure 2. Akt Phosphorylates Girdin In Vitro and In Vivo

(A) (Aa) A potential Akt phosphorylation site at serine 1416 of the Girdin CT domain. (Ab) Girdin CT-V5, WT or SA (serine 1416 replaced with alanine), was transfected into COS7 cells and immunoprecipitated with anti-V5 antibody, followed by incubation with recombinant active or inactive Akt in the presence of [γ-^{32}P]ATP. Phosphorylated Girdin CT was detected by autoradiography (upper panel). Immunoprecipitated Girdin CTs were detected by Western blot analysis (lower panel).

(B) Various fragments of Girdin (Ba) tagged with V5 were transfected into COS7 cells and immunoprecipitated with anti-V5 antibody, followed by (Bb) incubation with recombinant active Akt in the presence of [γ-^{32}P]ATP. Phosphorylated Girdin CT was detected by autoradiography (right panel). Immunoprecipitated fragments were detected by Western blot analysis (left panel).

(C) COS7 cells were cotransfected with Girdin CT-V5 (WT or SA) and Akt mutants. Immunoprecipitates with anti-V5 antibody were subjected to Western blot analysis with anti-phospho Girdin (anti-P-Girdin) antibody (upper panel). Expression of Girdin CTs and Akt mutants was monitored by Western blot analyses (middle and lower panels).

(D) COS7 cells were stimulated with EGF (50 ng/ml) for 15 min in the presence of DMSO (0.1%), PD98059 (50 μM), LY294002 (10 μM), and Wortmannin (30 nM). Immunoprecipitates with anti-Girdin antibody were subjected to Western blot analyses with anti-P-Girdin and anti-Girdin antibodies. Activation of Akt was monitored by Western blot analyses with anti-phospho Akt antibody.

(E) COS7 cells were transfected with Akt mutants. Endogenous Girdin was immunoprecipitated with anti-Girdin antibody, followed by Western blot analyses with anti-P-Girdin (upper panel) and anti-Girdin (lower panel) antibodies.

(F) Effects of Akt knockdown on phosphorylation of endogenous Girdin. (Fa) COS7 cells were transfected with either control or Akt siRNAs and were incubated for 48 hr. Cells were then stimulated with EGF (50 ng/ml) for 30 min, and the phosphorylation of Girdin was analyzed as described in (E). (Fb) Depletion of Akt in COS7 cells by siRNA.

the cells transfected with Akt small interfering RNA (Akt siRNA) (Figure 2F). These findings confirmed that Akt activation is necessary for Girdin phosphorylation.

Girdin Associates with Actin Filaments via Its C-Terminal Domain

To determine the subcellular localization of Girdin, we immunofluorescently stained Vero fibroblasts with the anti-Girdin Ab. The results showed that Girdin was co-localized with the actin stress fibers in quiescent cells (Figure 3Aa). When the cells were stimulated with EGF (50 ng/ml), they started to polarize, followed by directional extension of lamellipodia. In the EGF-stimulated cells, Girdin localized not only on the actin stress fibers, but also on the lamellipodia at the leading edge, which was illustrated upon staining for the Arp2/3 binding protein Cortactin (Figure 3Ab).

The localization of Girdin raises the possibility that Girdin is an F-actin (filamentous actin) binding protein. To identify the actin binding domain of Girdin, we generated green fluorescence protein (GFP)-fused, truncated versions encoding the NT (GFP-NT), the N-terminal half (GFP-M1) and the C-terminal half (GFP-M2) of the coiled-coil domain, and the N-terminal half (GFP-

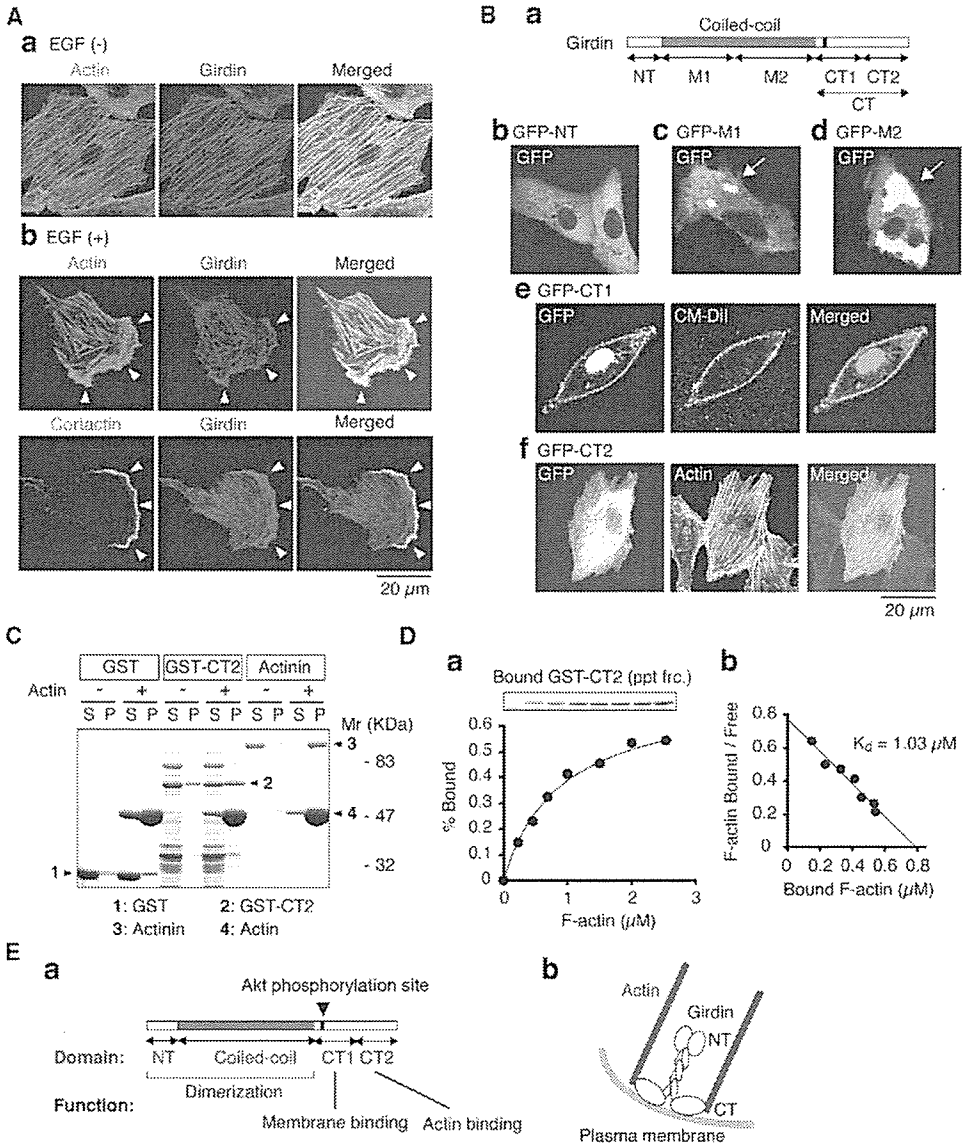

Figure 3. Girdin Binds to Actin Filaments through Its C-Terminal Domain

(A) (Aa) Quiescent or (Ab) EGF (50 ng/ml)-stimulated Vero cells were doubly stained with either Alexa488-phalloidin (upper panel) or anti-Cortactin antibody (lower panel) and anti-Girdin antibody. Arrowheads denote lamellipodia at the leading edge.

(B) Subcellular localization of Girdin fragments. Various fragments of Girdin (Ba) fused with GFP were expressed in Vero cells, fixed, and stained with the (Bb–Bf) indicated probes. Arrows denote aggregates of the expressed proteins. CM-DiI, Chloromethylbenzamido.

(C) Girdin CT2 directly interacts with filamentous actin in vitro. Purified GST (1), GST-CT2 (2), and α-actinin (3) were incubated with (+) or without (–) in vitro-prepared actin filaments (4). F-actin was subsequently pelletted by ultracentrifugation. Cosedimentation of the various proteins with F-actin was analyzed by CBB staining of the gel.

(D) Direct plot of binding of GST-CT2 to F-actin. A fixed amount of GST-CT2 (1 μM) was mixed with various amounts of F-actin (0–2.5 μM), followed by ultracentrifugation. Amounts of the free and bound GST-CT2 were quantified, and the (Da) percentage of bound GST-CT2 was plotted against the concentration of F-actin, and the (Db) K_d value was calculated by Scatchard analysis.

(E) (Ea) Summary of the localization and functions of Girdin domains. (Eb) The proposed structure of Girdin.

CT1) and the C-terminal half (GFP-CT2) of the CT domain, and we examined their intracellular localization (Figure 3Ba). When expressed in Vero cells, the GFP-NT, GFP-M1, and GFP-M2 localized in the cytoplasm (Figures 3Bb–3Bd). The GFP-CT1 localized in both the nucleus and the plasma membrane, as shown by its colocalization with CM-DiI, a carbocyanine membrane probe (Figure 3Be), while GFP-CT2 apparently localized on the stress fibers (Figure 3Bf). These findings suggest that Girdin localizes on the actin filament via its CT2 domain, whereas it also associates with the plasma membrane via its CT1 domain. The nuclear localization of the GFP-CT1 seen here may be an artifact, because no accumulation of endogenous Girdin was visible in the nucleus (Figure 3A).

We next investigated the actin binding properties of the CT2 domain by actin cosedimentation assays (Figures 3C and 3D). The purified glutathione S-transferase (GST)-fused CT2 (GST-CT2) cosedimented with purified F-actin, as did α-actinin, whereas GST alone did not

(Figure 3C), indicating that GST-CT2 directly binds to F-actin. As the amount of F-actin increased, the binding of GST-CT2 with F-actin was saturated (Figure 3Da). The estimated dissociation constant (K_d) for F-actin was 1.03 μM, indicating that Girdin has relatively low affinity for F-actin (Figure 3Db).

The domains of Girdin, their predicted functions, and the speculated structure of Girdin are summarized and illustrated in Figure 3E. Together, these findings allow us to propose that Girdin may possess an actin cross-linking property.

Girdin Is Required for the Formation of Actin Stress Fibers and Cell Migration

To assess the function of Girdin, we employed RNA-mediated interference (RNAi) to suppress (knockdown) the expression of Girdin in Vero cells. We introduced several Girdin small (21 nucleotide) interfering RNAs (Girdin siRNA) and a 21 nucleotide irrelevant RNAs (control siRNA) into Vero cells. Western blot analyses showed that transfection with the Girdin siRNAs effectively reduced the expression levels of Girdin by over 90% without affecting those of Akt and actin (Figure 4A). In order to verify the specificity of the knockdown experiments, the two oligonucleotides, Girdin siRNAs A and B, were utilized for Western blot analyses and other functional assays described in this study.

To test whether Girdin functions to promote the crosslinking of actin filaments, we examined the effects of Girdin knockdown on the organization of the actin cytoskeleton. Immunofluorescent staining with anti-Girdin Ab showed that the expression of Girdin was very low in the Girdin siRNA-transfected cells (Figure 4Bb). Staining of F-actin-rich structures with phalloidin revealed that the stress fibers were disrupted in the Girdin siRNA-transfected cells (Figure 4Bb), indicating that Girdin is essential for the formation of the stress fibers. When observed under higher magnification, Girdin siRNA-transfected cells contained markedly reduced thin and short stress fibers. Moreover, they lost their shape and formed with rugged boundaries that gave rise to the formation of multiple protrusions (leading edge) (Figure 4Bb, lower panel, and Figure 4C).

To further clarify the roles of Girdin in actin dynamics, we observed the behavior of the Girdin-depleted cells during migration in in vitro wound-healing assays (Figure 4D and Movies S1 and S2). We found that the Girdin siRNA-transfected cells facing the wound failed to produce extended lamellipodia at the leading edge and showed a migration defect that included multiple protrusions that were repeatedly stretched and shortened (Figure 4Db and Movie S2). These results suggest that Girdin is essential for organization of actin filaments during cell migration.

To test the specificity of the effect of the Girdin knockdown, we also introduced the Girdin siRNA into another cell line, SK-N-MC neuroblastoma cells, which stably express the RET receptor tyrosine kinase (Takahashi, 2001). Girdin siRNA-transfected SK-N-MC (RET) cells exhibited disruption of the stress fibers and limited formation of lamellipodia in response to the RET ligand, glial cell line-derived neurotrophic factor (GDNF) (Figure S3).

Localization of Girdin on Actin Filaments and Ultrastructure of the Girdin-Depleted Cells by Electron Microscopy

To further confirm the direct interaction of Girdin with actin filaments in vivo and its roles in actin organization, ultrastructural analysis was performed by deep-etch electron microscopy of "unroofed" Vero cells (Figure 5). Immunogold labeling revealed that Girdin molecules localize with actin filaments (Figure 5A). Higher-magnification views showed extensive colocalization of Girdin with the junctions between the actin filaments (Figure 5B).

Consistent with the immunofluorescence analysis, the density of the cortical actin filaments visible in electron micrographs of the cytoplasmic surface under the plasma membrane of Girdin-depleted Vero cells is lower than that in the control cells, where more tightly organized actin fibers predominate (Figure 5C). In the control siRNA-transfected cells, the filaments abut one another, run together without separating, and form thick cables tightly crosslinked by many molecules. Some filaments were oriented perpendicular to the other actin cables, resulting in interwoven and dense actin networks. In the Girdin siRNA-transfected cells, however, the actin bundles are sparse, and each actin filament is separated from another and is sometimes disrupted en route.

Phosphorylated Girdin Localizes to the Leading Edge of Migrating Cells

To gain insight into the role of Girdin phosphorylation by Akt, we examined the location of phosphorylated Girdin in Vero cells by staining with the anti-P-Girdin Ab (Figure 6A). In serum-starved quiescent cells, phosphorylation of Girdin was hardly detected throughout the cells (Figure 6A, top panel), consistent with the results of Western blot analyses (Figure 2D). When cells were stimulated with EGF (50 ng/ml), the immunostaining showed that phosphorylated Girdin appeared in the lamellipodia at the leading edge of migrating cells (Figure 6A, middle panel). The phosphorylated Girdin was also colocalized with Cortactin that exists at the leading edge (Figure 6B). Moreover, we observed that the stimulation of Vero cells with EGF enhanced the specific accumulation and localization of active Akt with phosphorylated Girdin in lamellipodia at the leading edge (Figure S4). In the Girdin siRNA-transfected cells, stimulation by EGF induced multiple leading edges. At these leading edges, the signals of phosphorylated Girdin were abolished as expected (Figure 6A, bottom panel), further supporting the specificity of the immunostaining. The nuclear signal seen in the immunostaining was still visible in the Girdin siRNA-transfected cells (Figure 6A, bottom panel), indicating that it was an artifact.

Akt Regulates the Association of Girdin with the Plasma Membrane

What is the mechanism that determines localization differences between the phosphorylated and nonphosphorylated forms of Girdin? Because the CT1 domain of Girdin localizes to the plasma membrane and contains the phosphorylation site, we hypothesized that it is the association of Girdin with the plasma membrane

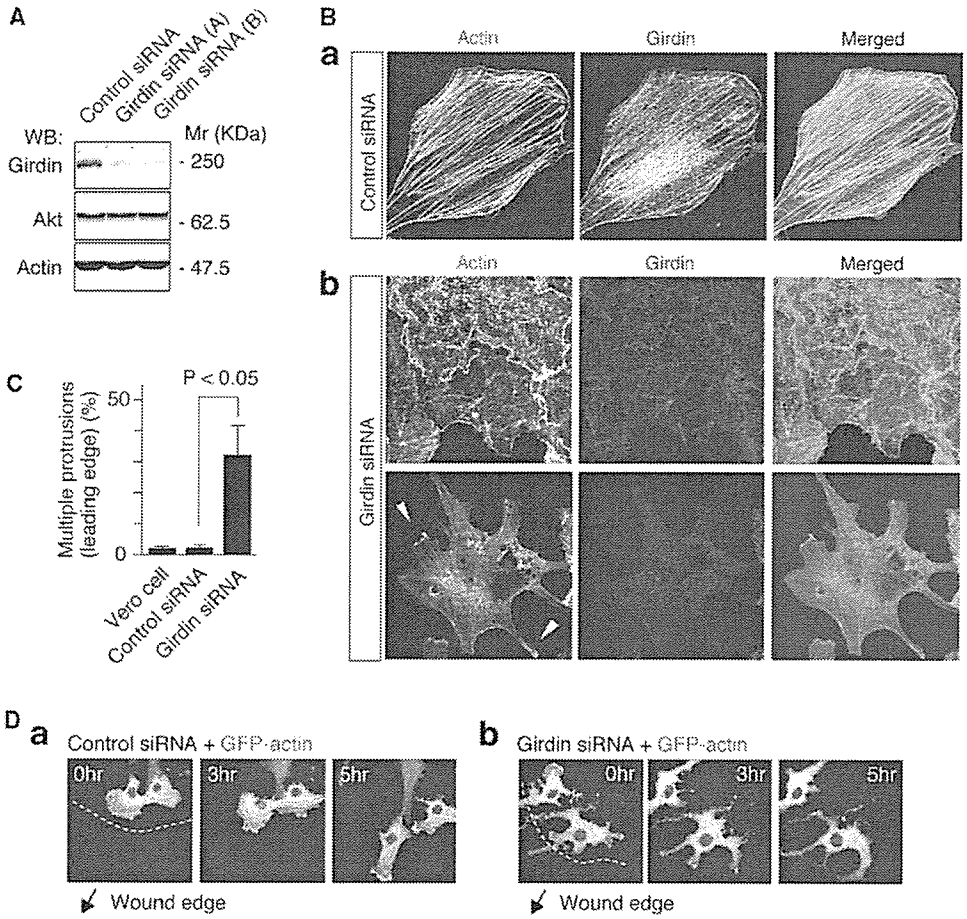

Figure 4. Girdin Is Essential for the Formation of Stress Fibers and Cell Migration

(A) Depletion of Girdin in Vero cells by siRNA. Total cell extracts from control siRNA- and Girdin siRNA-transfected Vero cells were subjected to Western blot analyses with anti-Girdin, anti-Akt, and anti-actin antibodies.

(B) Vero cells were transfected with (Ba) control or (Bb) Girdin siRNAs and fixed 72 hr after transfection, followed by staining with Alexa488-phalloidin and anti-Girdin antibody. Arrowheads denote lamellipodia at the tips of protrusions.

(C) After transfection of each siRNA, the number of cells with multiple protrusions was counted by staining with anti-Girdin antibody and Alexa488-phalloidin. More than 100 transfected cells were counted in each group. The results represent the means ± SE.

(D) Vero cells were cotransfected with GFP-actin and either (Da) control or (Db) Girdin siRNA and incubated for 48 hr. Cells were plated on fibronectin-coated glass coverslips and wounded to induce cell migration. Images were collected every 90 s for a period of 5–6 hr starting 2 hr after scraping. The arrows indicate the direction of cell migration into the wounds.

that is regulated by the phosphorylation. We found that a positively charged sequence of 19 amino acid residues (Arg-1389 to Lys-1407) upstream of the phosphorylation site (Figure 6Ca) resembles a consensus sequence for phosphatidylinositol 4,5-bisphosphate (PI[4,5]P2) binding (Sechi and Wehland, 2000). When the GFP-CT1 in which the phosphoinositide binding site was deleted (termed GFP-CT1 ΔPB) was transfected into Vero cells, localization of GFP-CT1 ΔPB to the plasma membrane was not observed (Figure 6Cb). This finding suggested that the CT1 domain is anchored at the plasma membrane through binding to phosphoinositides.

To examine the phosphoinositide binding properties of Girdin, we performed a protein-lipid binding assay with purified GST fusion proteins containing the phosphoinositide binding site of Girdin (Figures 6D and 6E). In the experiment, we utilized the CT domain fused with GST instead of the CT1 domain (Figure 6Da), because the GST-CT1 fusion protein was easily degraded during expression and purification procedures. As shown in Figure 6Ea, GST-CT bound selectively to PI(4)P and weakly to PI(3)P, but to none of the other phosphoinositides or phospholipids. The binding property of GST-CT to PI(4)P and PI(3)P was abrogated when the phosphoinositide binding site was deleted (Figure 6Eb). We also found that mutants of the CT1 domain, in which the positively charged basic residues were replaced with alanines (Girdin PBala mutant), failed to bind to the phosphoinositides and were delocalized from the plasma membrane (Figure S5), suggesting that the positive electrostatic charge generated by the basic residues in the phosphoinositide binding motif is required for the association of Girdin with the plasma membrane.

Since the phosphoinositide binding site is located near the Akt phosphorylation site (Figure 6Ca), the sup-

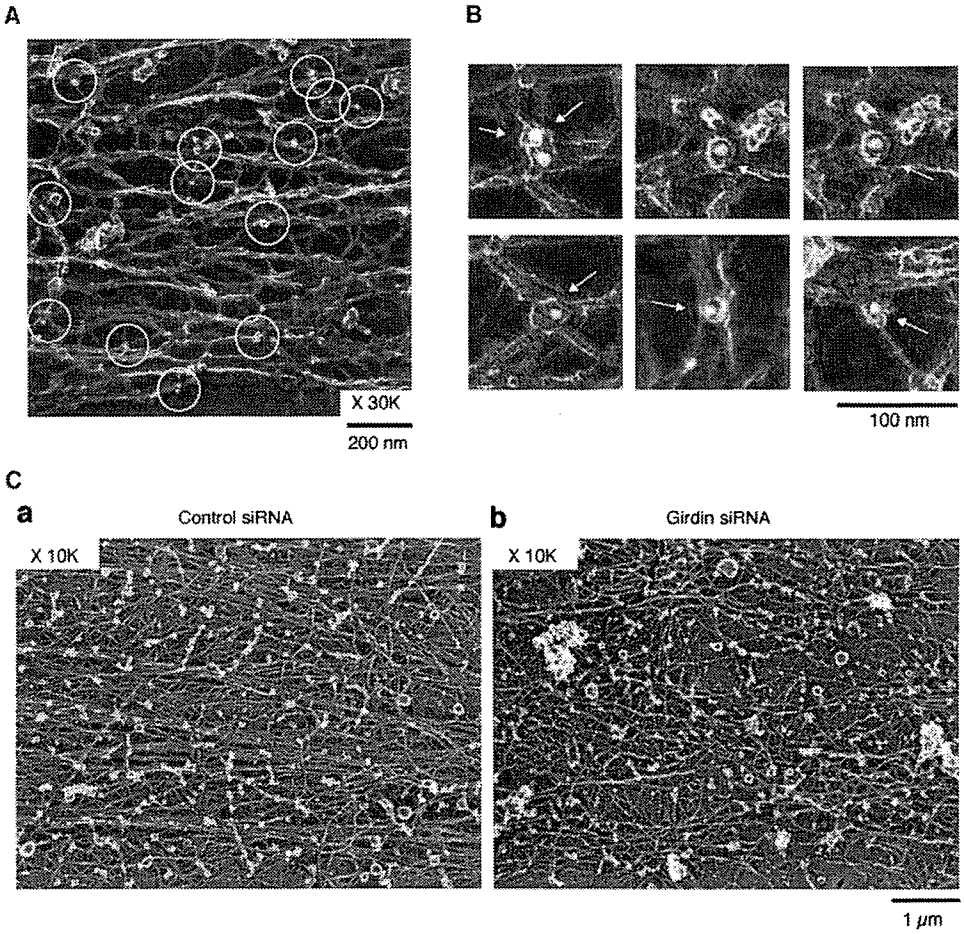

Figure 5. Electron Microscopic Analysis of Girdin Localization and the Effect of Its Depletion on Actin Organization

(A) Immunogold electron microscopy with anti-Girdin antibody.

(B) Circles indicate the immunogold signals of Girdin molecules, shown here under higher magnification. Arrows denote the immunogold signals.

(C) Ultrastructure of actin filaments in Vero cells transfected with either (Ca) control or (Cb) Girdin siRNA.

position was made that Akt might control the localization of Girdin by regulation of its phosphoinositide binding property. To determine if this is the case, we examined the phosphoinositide binding property of phosphorylated GST-CT. Purified GST-CT was effectively phosphorylated by Akt in vitro (Figure 6Db). GST-CT was then subjected to the protein-lipid binding assay, in which binding was detected by anti-P-Girdin Ab. As shown in Figure 6Ec, the phosphorylated GST-CT bound to neither PI(4)P nor PI(3)P. In addition, actin cosedimentation assays showed that the phosphorylation of GST-CT did not attenuate its affinity for F-actin (Figure 6F), and that the binding kinetics was similar to that of GST-CT2 (Figure 3D). These findings suggested that the binding of Girdin to the phosphoinositides, but not to F-actin, is attenuated by phosphorylation.

Moreover, we investigate whether the membrane association of Girdin is regulated by EGF treatment, by using COS7 cells expressing either the GFP-full-length Girdin WT or SA mutant. The results supported the view that phosphorylation at Ser-1416 by Akt is necessary for the delocalization of Girdin from the plasma membrane. (Figure S6).

Phosphorylation of Girdin by Akt Is Required for Cell Migration

The localization of phosphorylated Girdin at the leading edge prompted us to test whether the phosphorylation of Girdin is involved in cell motility. After wounding a confluent monolayer of Vero cells, immunostaining with anti-P-Girdin Ab showed that the level of Girdin phosphorylation in cells at the wound edge increased soon after scratching, reached a maximum at 8 hr, and lasted for at least 12 hr (Figure 7A). The implication is that the phosphorylation of Girdin may play an important role in cell motility. Thus, the role of Girdin in cell motility was examined with Boyden chamber assays. The Girdin knockdown significantly retarded the ability of Vero cells to migrate in response to EGF (50 ng/ml) added to the lower chamber (Figure 7B). We also found that expression of the CT domain in Vero cells significantly attenuated cell migration (Figure 7B), supporting the

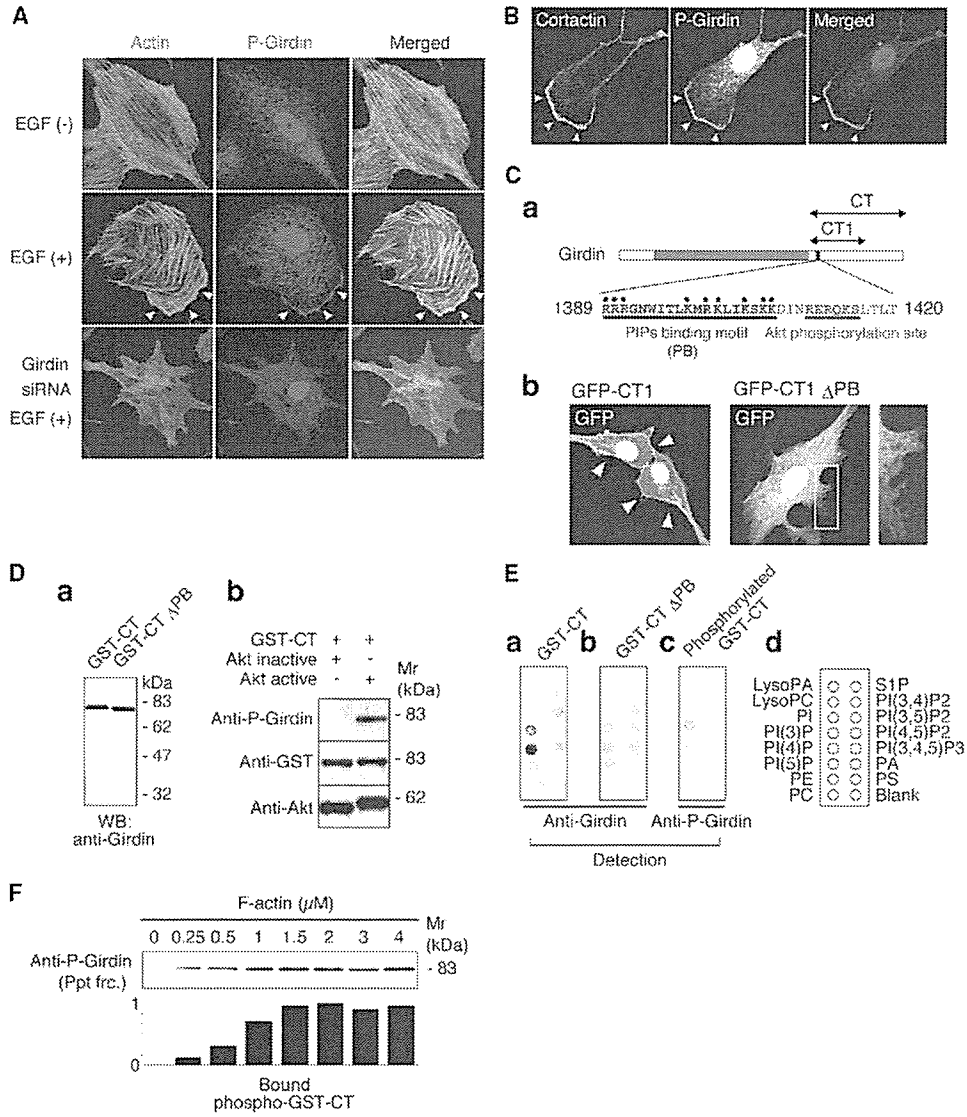

Figure 6. Effects of Girdin Phosphorylation on Its Localization and Interaction with Phosphoinositides

(A) Quiescent (upper panel), EGF (50 ng/ml)-stimulated (middle panel), and Girdin siRNA-transfected (lower panel) Vero cells were fixed and stained with Alexa488-phalloidin and anti-phospho Girdin (P-Girdin) antibody. Arrows denote the lamellipodia where the phosphorylated Girdin accumulates.

(B) Migrating Vero cells were stained with anti-Cortactin and anti-P-Girdin antibody.

(C) (Ca) The putative phosphoinositide binding site (PB) upstream of the Akt phosphorylation site in Girdin is indicated. (Cb) Vero cells were transfected with either GFP-CT1 (left) or GFP-CT1 in which the phosphoinositide binding site was deleted (GFP-CT1 ΔPB) (right). Arrows denote GFP signals at the plasma membrane.

(D) Purification of GST-CT and protein-lipid overlay assays. (Da) Purified GST-CT and GST-CT ΔPB were analyzed by Western blotting with anti-Girdin antibody. (Db) Phosphorylation of purified GST-CT by recombinant Akt in vitro. The phosphorylated GST-CT in an in vitro kinase assay was detected with anti-P-Girdin antibody.

(E) Protein-lipid overlay assays with (Ea) GST-CT, (Eb) GST-CT ΔPB, and the (Ec) phosphorylated GST-CT. The lipid binding of both GST-CT and GST-CT ΔPB was detected with anti-Girdin antibody, whereas that of phosphorylated GST-CT was detected with anti-P-Girdin antibody. (Ed) The various lipids spotted on the membrane (100 pmol lipid per spot) are indicated. PA, phosphatidic acid; PC, phosphocholine; PI, phosphatidylinositol; PE, phosphatidylethanolamine; PS, phosphatidylserine; S1P, sphingosine-1-phosphate.

(F) Binding of phosphorylated Girdin CT to F-actin. GST-CT was phosphorylated by Akt in vitro (Db) and subjected to an actin cosedimentation assay. A fixed amount of GST-CT (1 μM) was phosphorylated in vitro and mixed with various amount of F-actin (0–4 μM), followed by ultracentrifugation. The amount of phosphorylated GST-CT bound to F-actin in the pellet fraction (Ppt frc.) was monitored by Western blot analyses with anti-P-Girdin antibody.

notion that the interaction of endogenous Girdin with actin filaments is important for integral cell migration. Consistent with previous studies (Higuchi et al., 2001; Kim et al., 2001), the depletion of Akt by siRNA also attenuated the migration (Figure 7B), which suggests that intrinsic Akt activity is requisite for Vero cells to migrate through the pores in this assay system.

To next examine whether adding Girdin exogenously

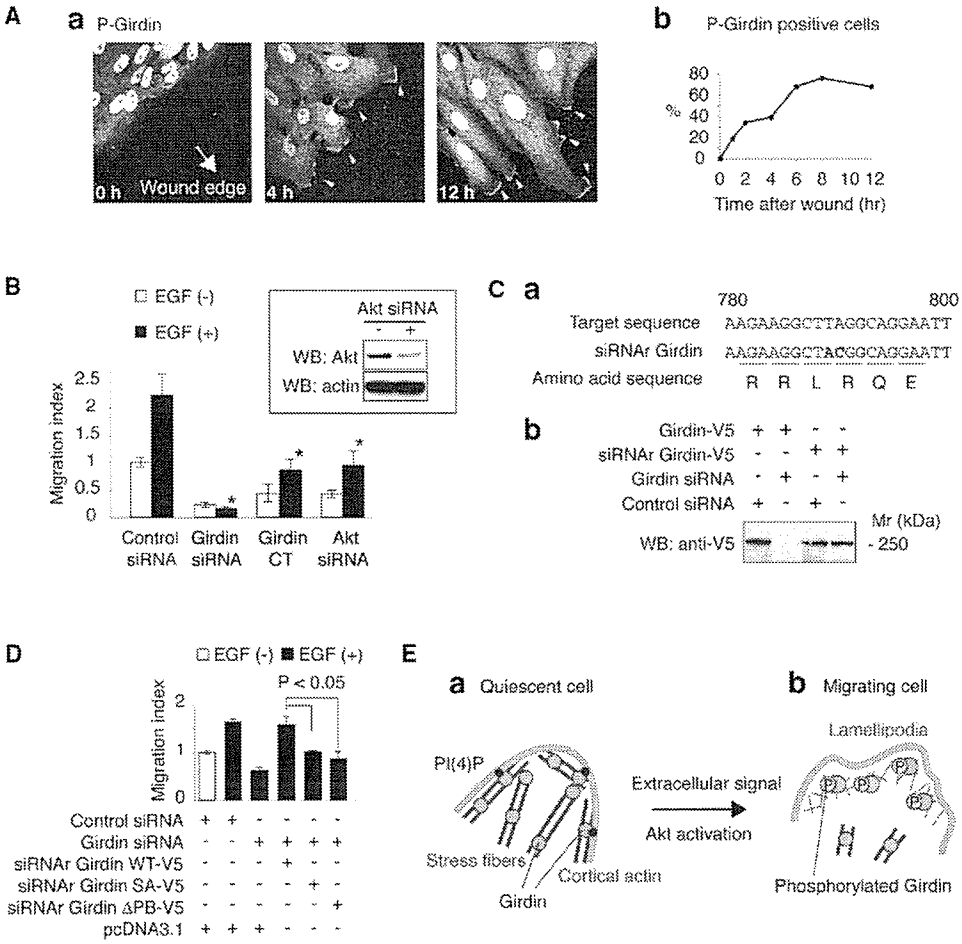

Figure 7. Phosphorylation of Girdin Regulates Cell Migration

(A) Girdin is phosphorylated at the leading edge during cell migration. (Aa) After scratching a monolayer of Vero cells, the cells facing the wound were fixed and stained with anti-P-Girdin antibody. Arrowheads denote the signals of the phosphorylated Girdin. (Ab) The phosphorylation of Girdin localizing at the leading edge increases in a time-dependent fashion.

(B) Vero cells were transfected with GFP (0.5 μg) and either siRNA (20 pmol) or Girdin CT (2.5 μg), incubated for 48 hr, and subjected to Boyden chamber assays in the presence or absence of EGF (100 ng/ml) in the lower chamber. Asterisks indicate statistical significance (Student's t test; *$p < 0.05$) compared with control. The inset shows the depletion of Akt in Vero cells by siRNA. The results represent the mean ± SE.

(C) Generation of an siRNA-resistant (siRNAr) mutant of Girdin. (Ca) The target sequence of Girdin siRNA ("B" in Figure 4A) and the nucleotide substitution for the generation of the siRNAr version are indicated. (Cb) Cell lysates from COS7 cells cotransfected with indicated siRNAs and constructs were analyzed by Western blotting with anti-V5 antibody.

(D) Vero cells were cotransfected with GFP (0.5 μg), siRNAs (20 pmol), and indicated constructs (2.5 μg), incubated for 48 hr, and subjected to Boyden chamber assays. Expression levels of Girdin mutants in cells prior to plating for migration assays were monitored by Western blot analysis with anti-V5 antibody and were found to be similar (data not shown). The results represent the mean ± SE.

(E) A proposed model for the regulation of cell motility by the phosphorylation of Girdin. In (Ea) quiescent cells, Girdin crosslinks actin filaments and anchors cortical actin at the plasma membrane, whereas during (Eb) cell migration, Akt-mediated phosphorylation allows Girdin to localize at the leading edge and contribute to the formation of short-branched filaments in the lamellipodium.

restores the defect in cell migration observed in the knockdown cells, we constructed siRNA-resistant (siRNAr) versions of Girdin harboring silent mutations (Figure 7C). As shown in Figure 7D, the expression of the siRNAr-Girdin WT fully restored migratory response to EGF. In contrast, the expression of the siRNAr-Girdin mutants in which the Ser-1416 was mutated to Ala (siRNAr-Girdin SA), the phosphoinositide binding site was deleted (siRNAr-Girdin ΔPB), or the basic residues in the phosphoinositide binding site were replaced with alanines (siRNAr-Girdin PBala) failed to complement the migration defect (Figure 7D and Figure S5C). We also confirmed these findings by performing migration assays with a human fibrosarcoma cell line, HT-1080 (Figure S7).

Finally, we directly examined the movement of Vero cells expressing the Girdin mutants by wound-healing assays (Figure S8 and Movies S3–S6). Cells expressing Girdin WT effectively and rapidly moved into the wound (Movie S3), but those expressing Girdin SA exhibited elongated shape. Moreover, the location of the nuclei of the latter cells seemed to be fixed and motionless, suggesting that the cells could not undergo detachment from the matrix (Movie S4). Cells expressing Gir-

din ΔPB and Girdin PBala were less locomotive compared with those expressing Girdin WT (Movies S5 and S6, respectively). These results demonstrate that expression of the Girdin mutants impairs proper directional cell migration. Considered with the findings shown in Figure 6 and Figure S6, these data indicate that the regulation of an interaction between Girdin and the plasma membrane by Akt is crucial for cell migration.

Discussion

The Structure of Girdin/APE and Its Roles in Actin Organization

In a search for molecules that interact with Akt, we have identified a novel, to our knowledge, actin binding protein, designated Girdin/APE, that is essential for actin organization. Four different regions can be distinguished in the Girdin molecule based on the sequences of its subunits, subcellular localization, and functions: an N-terminal region that seems to facilitate the formation of a dimer (NT), an extremely long coiled-coil region, a region that binds to the plasma membrane through the interaction with phosphoinositides (CT1), and a C-terminal region that encompasses an actin binding site (CT2). The amino acid sequence of the CT2 domain shows no homology with the calponin homology (CH) domain, a common actin binding domain that is present in most actin binding proteins such as α-actinin, filamins, fimbrin, spectrins, cortexillins, and dystrophin (Gimona et al., 2002), suggesting that Girdin represents a novel class of actin binding proteins.

Analysis of the sequence of Girdin reveals that it includes 135 heptad repeats, $(abcdefg)_{135}$, between Leu-253 and Lys-1375 that correspond to a central rod domain. Within the repeats, positions *a* and *d* are preferentially occupied by hydrophobic residues like Leu, Ile, Met, or Val (Figure S1), which is consistent with the signature of canonical coiled-coil structures that wind around each other in a superhelix (Cohen and Parry, 1994). The oligomerization properties of coiled-coil sequences are determined by the distribution of β-branched residues in the *a* or *d* positions (Harbury et al., 1993; Faix et al., 1996). Val and Ile in *a* favor dimerization, they favor tetramerization in *d*, and their presence in both *a* and *d* facilitates the formation of trimers. In the coiled-coil sequence of Girdin, 22 repeats have Val or Ile in the *a* position, whereas they are present in the *d* position of only 9 repeats, suggesting that the coiled-coil domain of Girdin tends to form a dimer. This is consistent with our findings suggested by gel filtration that the NT domain of Girdin forms a dimer (Figure S2).

It has been established that the possession of two actin binding sites enables crosslinking or bundling proteins to link filaments and to stabilize higher-order assemblies of actin filaments (Pollard, 2002). Possessing two actin binding CT2 domains in juxtaposition, the dimeric Girdin molecules seem to be designed to gather actin filaments together into bundles or a meshwork. Consistent with this possibility are the findings of immunofluorescent staining and electron microscopy that the depletion of Girdin interfered with actin networks, leading to the disruption of stress fibers, cortical actin filaments, and actin meshwork at the leading edge. During migration, the Girdin knockdown cells produced multiple protrusions, resulting in limited directional migration. These observations indicate that Girdin fulfils an essential function in determining the stability and integrity of actin bundles and meshwork that mediates a variety of important biological processes. Eukaryotic cells have a fail-safe mechanism in the multiple actin crosslinking proteins that share overlapping functions (Pollard, 2002). The phenotypic consequences of the depletion of Girdin indicate that the presence of other proteins cannot completely compensate for its loss. Because the speculated primary structure, molecular size, and putative function of Girdin are reminiscent of those of filamin (Stossel et al., 2001), it is important to clarify the functional difference and synergism between the two.

We found that the CT1 domain of Girdin associates with the plasma membrane through the cluster of basic amino acid residues Arg-1389 to Lys-1407. This positively charged sequence is related to a consensus sequence for PI(4,5)P2 binding, which has been found in gelsolin, villin, profilin, vinculin, and other various cytoskeletal proteins (Janmey et al., 1992). Unexpectedly, our experiment showed that the basic amino acid cluster in Girdin does not bind to PI(4,5)P2, but binds to PI(4)P and binds weakly to PI(3)P. Considering that PI(4)P, but not PI(3)P, is abundant in mammalian cells (Vanhaesebroeck et al., 2001), it is plausible to conclude that Girdin binds to PI(4)P, which resides in the membranes of mammalian cells in an amount equal to that of PI(4,5)P2. We speculate that it stabilizes the cortical actin filaments by anchoring them at the plasma membrane.

Roles of Girdin and Its Regulation in Cell Motility

Relatively little is known about how cells regulate actin crosslinking proteins in response to external stimuli (Pollard, 2002; Small et al., 2002). In the present study, we found that Akt phosphorylates Girdin in vitro and in intact cells. The phosphorylation of Girdin was induced by EGF and during cell migration, suggesting a significance for phosphorylation in physiological cellular events. In migrating Vero fibroblasts, the phosphorylated Girdin preferentially localizes to lamellipodia at the leading edge, which is in line with our and previous observations that activated Akt is also localized at the leading edge during migration in mammalian cells (Higuchi et al., 2001; Kim et al., 2001; Figure S4). It is plausible that Akt, activated downstream of PI3K, translocates from the cytosol to the leading edge through its PH domain, and subsequently phosphorylates Girdin on the actin filaments at the front of the cells.

How does Akt regulate the function of Girdin by phosphorylation? Insight into this issue comes from our observation that the phosphorylation of the CT domain of Girdin affects in vitro binding to PI(4)P. Because the phosphorylation site is present in the neighborhood of the phosphoinositide binding site, it is speculated that phosphorylation induces a conformational change around these sites, and this change in turn alters affinity for the phosphoinositide. We further found that the phosphorylated CT domain retains the property of actin

binding, and its affinity for F-actin is comparable to that of the nonphosphorylated form. Based on these observations, we speculate that phosphorylation by Akt releases Girdin from PI(4)P and allows it to localize at the leading edge in order to crosslink the newly generated actin filaments in the lamellipodium network, as illustrated in Figure 7E.

The leading lamellipodium of motile cells is a sheet-like protrusion filled with actin filaments at high density (Small et al., 2002). Because long and flexible actin filaments cannot sustain a pushing force (Pollard and Borisy, 2003), cells must create a dense array of short-branched filaments by utilizing crosslinking proteins, which allow nascent filaments to push against the membrane at the leading edge. The major crosslinking components at lamellipodium are filamin and α-actinin (Small et al., 2002). Cells derived from human malignant melanomas lacking filamin had unstable lamellipodia and exhibited impaired locomotion (Stossel et al., 2001). *Dictyostelium* cells lacking both α-actinin and ABP-120 (the filamin homolog) showed motility defects (Rivero et al., 1996). Both of these proteins have a relatively low affinity for actin filaments, with K_d values in the micromolar range. This low affinity enables their rapid binding and dissociation with the filaments and allows networks of actin filaments to passively change shape when prolonged force is applied while resisting rapid deformations (Pollard, 2002). This is also the case with Girdin, which has a low affinity for F-actin, with a K_d value of ~1 μM. An important goal is to reveal functional divergence and structural complementation between Girdin and other crosslinking proteins in the lamellipodium.

The role of Girdin in cell migration is supported by the findings that Girdin knockdown cells migrated poorly and exhibited insufficient lamellipodium formation at their leading edge. However, they revert to normal behavior when siRNAr-Girdin is added. In contrast, cells expressing siRNAr-Girdin SA, ΔPB, and PBala mutants exhibited limited migration (Figure 7, Figure S8, and Movies S3–S6). As Girdin SA may be constantly anchored at the plasma membrane without undergoing phosphorylation, and Girdin ΔPB and PBala do not associate with the plasma membrane (Figure S6), our findings suggest that spatially selective regulation of Girdin phosphorylation by Akt at the cytoplasm-membrane interface is essential for reorganization of the actin cytoskeleton.

Activation of Akt is correlated with an increase in cell migration and invasion in several mammalian systems. The overexpression of active Akt promotes cell motility in mammalian cells such as fibroblasts, fibrosarcoma cells, and vascular endothelial cells (Higuchi et al., 2001; Kim et al., 2001; Morales-Ruiz et al., 2000). Rac and Cdc42, small GTPases essential for lamellipodia formation and establishment of cell polarity, activate Akt at the leading edge of fibroblasts (Higuchi et al., 2001). Akt is involved in the trafficking and recycling of vitronectin and fibronectin receptors (αvβ3 and α5β1 integrins, respectively), which regulate cell spreading and migration (Roberts et al., 2004). Finally, the association of Pak1 (p21-activated protein kinase) with Nck, an adaptor protein, is crucial for cell movement and is modulated by Akt (Zhou et al., 2003). Along with our present findings, these data indicate the involvement of Akt in cell motility. In addition, it was recently demonstrated that Akt and its substrate glycogen synthase kinase-3β (GSK-3β) are essential proteins in the determination of axon-dendrite polarity of neurons (Yoshimura et al., 2005; Jiang et al., 2005). Because the depletion of Girdin results in the formation of multiple leading edges and limited directional migration in Vero fibroblasts, the possible involvement of the Akt-Girdin pathway in the regulation of cell polarity should not be overlooked.

In conclusion, we demonstrated a novel, to our knowledge, role of Girdin/APE in actin organization and cell motility that is regulated by Akt. Anai et al. (2005) reported that Girdin/APE also functions as an enhancer of Akt and stimulates DNA synthesis. When Girdin/APE and Akt were overexpressed in cells, they found that cell proliferation was inhibited and apoptosis was induced. Thus, further investigation could shed light on important roles of Girdin/APE in different cellular processes.

Experimental Procedures

Yeast Two-Hybrid Assays

To identify proteins interacting with Akt, a full-length cDNA encoding human Akt1 was inserted into the pAS2 vector (Clontech). The resulting construct was used as bait to screen a human fetal brain MATCHMAKER cDNA library as previously described (Murakami et al., 2002). Two positive plasmids containing cDNA inserts were selected and sequenced. They contained the cDNA fragments encoding the C-terminal region of Girdin (residues 1217–1870). A full-length cDNA encoding Girdin was isolated from the human fetal brain poly A^+ RNA by 5′ rapid amplification of cDNA ends (5′-RACE system, Invitrogen). Additionally, we performed yeast two-hybrid binding assays with purified pAS and pACT constructs containing the fragments of human Akt1 and Girdin cDNAs.

Plasmids

Wild-type, constitutively active, and dominant-negative human Akt1 constructs were generously provided by Y. Gotoh (University of Tokyo). The constructs of pcDNA3.1-, pGEX-, and pEGFP-Girdin fragments were produced as described elsewhere (Murakami et al., 2002). EGFP was fused to the amino termini, and V5 and myc tags were fused to the carboxyl termini of the proteins. Girdin mutants were generated by using the QuikChange site-directed mutagenesis kit (Stratagene) according to the manufacturer's protocol. The siRNA-resistant Girdin was created by introducing two silent mutations into Girdin at nucleotides 780–800 (5′-AAGAAGGCTACGG CAGGAATT-3′) (underline indicates mutations).

Antibodies

Rabbit anti-Girdin polyclonal antibody was developed against the 19 carboxyl-terminal amino acids of Girdin and affinity-purified with the immunized peptide. The anti-phospho Girdin polyclonal antibody was supplied by Kumamoto Immunochemical Laboratory, Transgenic, Inc. (Kumamoto, Japan). It was raised by immunizing rabbits with a keyhole limpet hemocyanin-conjugated phosphopeptide corresponding to Girdin amino acid sequence 1408–1420 (CDINRERQKpSLTLT). Antiserum was purified as a bound fraction of the phosphopeptide-conjugated column.

Other antibodies used in this study include anti-Akt polyclonal antibody (Cell Signaling Technology), anti-phospho Akt polyclonal antibody (Cell Signaling Technology), and anti-Cortactin monoclonal antibody (Upstate).

Kinase Assays

Immunoprecipitates with anti-V5 antibody (Invitrogen) from COS7 cells expressing Girdin CT-V5 WT or SA or purified GST-CT were incubated with recombinant active or inactive Akt (500 ng) (Up-

state) with 10 μCi [γ-^{32}P]ATP (3000 Ci/mmol, Amersham) in kinase buffer (20 mM MOPS, 25 mM β-glycerophosphate, 5 mM EGTA, 15 mM $MgCl_2$, 1 mM dithiothreitol, and 1 mM $NaVO_3$). Mixtures were incubated at 30°C for 30 min, and reactions were terminated by the addition of Laemmli sodium dodecyl sulfate (SDS) sample dilution buffer (20 mM Tris-HCl [pH 6.8], 2 mM EDTA, 2% SDS, 10% sucrose, 20 μg/ml bromophenol blue, 80 mM dithiothreitol).

Immunofluorescent Staining

Vero cells were plated on fibronectin- (10 μg/ml, Sigma) and collagen I (10 μg/ml, Upstate)-coated coverslips or glass base dishes, fixed, and stained with the indicated antibodies. Fluorescence was examined by using a confocal laser-scanning microscope (Fluoview FV500, Olympus).

Actin Cosedimentation Assays

F-actin cosedimentation assays were performed according to the manufacturer's protocol (Cytoskeleton). Briefly, purified GST fusion proteins, GST alone, and α-actinin (Cytoskeleton) were incubated for 30 min at room temperature with 40 μg pure actin filaments. The final concentration of F-actin was 18 μM. Filaments were subsequently pelleted by centrifugation (100,000 × g) (Beckman). The cosedimented proteins were resolved by SDS-PAGE and detected by either Coomassie Brilliant Blue (CBB) staining or Western blot analyses with anti-GST antibody (Cell Signaling Technology) or anti-phospho Girdin Ab.

For quantitative analyses, a fixed concentration of GST-Girdin CT2 (1 μM) was mixed with increasing amounts of F-actin (0–2.5 μM) in polymerization buffer and incubated at room temperature for 30 min. Proteins were centrifuged as described above, and total pellets and supernatants were loaded separately on SDS-PAGE. Protein bands were detected by CBB staining and scanned and quantified with the software program WinROOF (Mitani Corp., Fukui, Japan).

RNA Interference

The siRNA-mediated knockdown of Girdin and Akt was performed by using previously described methods (Watanabe et al., 2004). The targeted sequences that effectively mediated the silencing of the expression of Girdin are as follows (only sense sequences are shown): 5′-AACCAGGTCATGCTCCAAATT-3′ (nucleotides 145–165, Girdin siRNA [A]) and 5′-AAGAAGGCTTAGGCAGGAATT-3′ (nucleotides 780–800, Girdin siRNA [B]). The 21 nucleotide synthetic duplexes were prepared by Qiagen. The siRNA specific to human Akt1 was purchased from Qiagen. Vero cells were transfected with the siRNAs or a 21 nucleotide irrelevant RNA (Qiagen) as a control, by using lipofectamine 2000 (Invitrogen) according to the manufacturer's protocol.

Freeze-Replica Electron Microscopy of the Cytoplasmic Cell Surface

Electron microscopy for the cytoplasmic surface of the cell membrane was carried out according to previously described methods (Heuser, 1989, 2000; Usukura, 1993). Vero cells cultured on glass coverslips (3 mm in diameter, standard #1 Matsunami, Osaka, Japan) were transfected with siRNAs. Immediately after being unroofed from the apical cell membrane, the cells were fixed for 30 min in 2.5% glutaraldehyde in buffer A (70 mM KCl, 5 mM $MgCl_2$, 3 mM EGTA, 30 mM HEPES buffer adjusted at pH 7.4 with KOH). After being washed with buffer A/distilled water, specimens were quickly frozen with liquid helium by using the rapid-freezing device (Eiko, Tokyo, Japan). Samples were then freeze etched and rotary shadowed with platinum-carbon, in a newly developed freeze etching device (FR9000, HITACHI, Ibaraki, Japan). For immunolabeling of Girdin molecules, the unroofed cells were fixed for 30 min in 4% paraformaldehyde/0.5% glutaraldehyde in buffer A. After being washed three times with buffer B (100 mM NaCl, 30 mM HEPES, 2 mM $CaCl_2$), the samples were quenched and blocked, and then labeled for 1 hr at 37°C with primary and secondary 10 nm gold-conjugated antibodies (Amersham) in buffer B containing 1% BSA. Finally, specimens were rapidly frozen and freeze etched as described above.

Scratch-Induced Cell Migration and Time-Lapse Imaging

Directional cell migration of Vero cells was stimulated in a monolayer by using an in vitro scratch wound assay (Watanabe et al., 2004). Vero cells were seeded on fibronectin-precoated coverslips or 35 mm glass base dishes and were transfected with indicated siRNAs. A total of 48 hr after the transfection, the confluent Vero cells were scratched with a 200 μl disposable plastic pipette tip and were allowed to migrate toward the wound. The cells were fixed at the indicated times for immunofluorescent staining. For time-lapse observation, cells were cotransfected with siRNAs and GFP-actin and were subjected to the scratch wound assays. The cells at the wound edges were observed with a confocal laser scanning microscope (Fluoview FV500, Olympus).

Three-Dimensional Cell Migration Assays

To assess the motility of cells transfected with various constructs or siRNAs, we performed the modified Boyden chamber migration assay, which enabled us to count GFP-labeled cells migrating across a fluorescence-blocking planer micropore membrane by using HTS FluoroBlok Insert (8.0 μm pores, 24-well format, Becton Dickinson). Both sides of the membrane were coated with 10 μg/ml fibronectin for 12 hr at 37°C and were washed with phosphate-buffered saline (PBS). The chambers were then placed in 24-well dishes filled with Dulbecco's modified Eagle's medium (DMEM) containing 0.1% BSA with or without 20 ng/ml human recombinant EGF. For migration assays of HT-1080 cells, DMEM with 10% fetal bovine serum (FBS) was added to the lower chamber. Cells (1 × 10^5) were transfected with GFP (0.5 μg, to identify transfected cells), indicated constructs (2.5 μg), and siRNAs (20 pmol) in 24-well plates, plated in the upper compartment, and allowed to migrate through the pores of the membrane for 4 hr. Cell motility was quantified by using a fluorescence microscope to count the GFP-positive cells that had migrated through the membrane.

Protein-Lipid Overlay Assays

GST fusion proteins were expressed in DH5α or BL21-CodonPlus (Stratagene) cells and purified by using conventional methods. Binding of the purified GST-CT to phospholipids was examined at 4°C by using a PIP-Strip (Echelon Bioscience) according to the manufacturer's protocol. Bound GST-CT proteins were detected with either anti-Girdin or anti-phospho Girdin antibodies.

Data Analysis

Data are presented as the mean ± SE. Statistical significance was evaluated by Student's t test.

Supplemental Data

Supplemental Data including eight figures, six movies, and Supplemental Experimental Procedures are available at http://www.developmentalcell.com/cgi/content/full/9/3/389/DC1/.

Acknowledgments

We thank Y. Gotoh (University of Tokyo) for providing Akt cDNAs and helpful discussion, T. Fukuda (Tohoku University) for helpful discussion, M. Nakayama (Nagoya University) for discussions on migration assays, K. Kadomatsu and K. Ichihara (Nagoya University) for providing HT-1080 cells, and N. Saka and A. Muraki (Nagoya University) for help in characterization of Girdin. This work was supported by Grants-in-Aid for Center of Excellence (COE) Research, Scientific Research (A), and Scientific Research on Priority Area "Cancer" from the Ministry of Education, Culture, Sports, Science and Technology of Japan (to M.T.). A.E. is a fellow of the Japan Society for the Promotion of Science.

Received: February 16, 2005
Revised: May 19, 2005
Accepted: August 3, 2005
Published: September 6, 2005

References

Alessi, D.R., Caudwell, F.B., Andjelkovic, M., Hemmings, B.A., and Cohen, P. (1996). Molecular basis for the substrates specificity of

protein kinase B; comparison with MAPKAP kinase-1 and p70 S6 kinase. FEBS Lett. *399*, 333–338.

Anai, M., Shojima, N., Katagiri, H., Ogihara, T., Sakoda, H., Onishi, Y., Ono, H., Fujishiro, M., Fukushima, Y., Horike, N., et al. (2005). A novel protein kinase B (PKB)/AKT-binding protein enhances PKB kinase activity and regulates DNA synthesis. J. Biol. Chem. *280*, 18525–18535.

Brazil, D.P., Park, J., and Hemmings, B.A. (2002). PKB binding proteins: getting in on the Akt. Cell *111*, 293–303.

Chung, Y., Potikyan, G., and Firtel, R.A. (2001). Control of cell polarity and chemotaxis by Akt/PKB and PI3 kinase through the regulation of PAKa. Mol. Cell *7*, 937–947.

Cohen, C., and Parry, D.A.D. (1994). α-helical coiled-coils: more facts and better prediction. Science *265*, 488–489.

Datta, S.R., Brunet, A., and Greenberg, M.E. (1999). Cellular survival: a play in three Akts. Genes Dev. *13*, 2905–2927.

Etienne-Manneville, S., and Hall, A. (2002). Rho GTPases in cell biology. Nature *420*, 629–635.

Faix, J., Steinmetz, M., Boves, H., Kammerer, R.A., Lottspeich, F., Mintert, U., Murphy, J., Stock, A., Aebi, U., and Gerisch, G. (1996). Cortexillins, major determinants of cell shape and size, are actin-bundling proteins with a parallel coiled-coil tail. Cell *86*, 631–642.

Gimona, M., Djinovic-Carugo, K., Kranewitter, W.J., and Winder, S.J. (2002). Functional plasticity of CH domains. FEBS Lett. *513*, 98–106.

Harbury, P.B., Zhang, T., Kim, P.S., and Alber, T. (1993). A switch between two, three and four stranded coiled-coils in GCN4 leucine zipper mutants. Science *262*, 1401–1407.

Heuser, J. (1989). Effect of cytoplasmic acidification on clathrin lattice morphology. J. Cell Biol. *108*, 401–411.

Heuser, J. (2000). The production of 'cell cortices' for light and electron microscopy. Traffic *1*, 545–552.

Higuchi, M., Masuyama, N., Fukui, Y., Suzuki, A., and Gotoh, Y. (2001). Akt mediates Rac/Cdc42-regulated cell motility in growth factor-stimulated cells and invasive PTEN knockout cells. Curr. Biol. *11*, 1958–1962.

Janmey, P.A., Lamb, J., Allen, P.G., and Matsudaira, P.T. (1992). Phosphoinositide-binding peptides derived from the sequence of gelsolin and villin. J. Biol. Chem. *267*, 11818–11823.

Jiang, H., Guo, W., Liang, X., and Rao, Y. (2005). Both the establishment and the maintenance of neuronal polarity require active mechanism: critical roles of GSK-3β and its upstream regulation. Cell *120*, 123–135.

Kim, D., Kim, S., Koh, H., Yoon, S., Chung, A., Cho, K.S., and Chung, J. (2001). Akt/PKB promotes cancer cell invasion via increased motility and metalloproteinase production. FASEB J. *15*, 1953–1962.

Lauffenburger, D.A., and Horwitz, A.F. (1996). Cell migration: a physically integrated molecular process. Cell *84*, 359–369.

Lupas, A., Van Dyke, M., and Stock, J. (1991). Predicting coiled coils from protein sequence. Science *252*, 1162–1164.

Meili, R., Ellsworth, C., Lee, S., Reddy, T.B., Ma, H., and Firtel, R.A. (1999). Chemoattractant-mediated transient activation and membrane localization of Akt/PKB is required for efficient chemotaxis to camp in *Dictyostelium*. EMBO J. *18*, 2092–2105.

Merlot, S., and Firtel, R.A. (2003). Leading the way: directional sensing through phosphatidylinositol 3-kinase and other signaling pathways. J. Cell Sci. *116*, 3471–3478.

Morales-Ruiz, M., Fulton, D., Sowa, G., Languino, L.R., Fujio, Y., Walsh, K., and Sessa, W.C. (2000). Vascular endothelial growth factor-stimulated actin reorganization and migration of endothelial cells is regulated via the serine/threonine kinase Akt. Circ. Res. *86*, 892–896.

Murakami, H., Yamamura, Y., Shimono, Y., Kawai, K., Kurokawa, K., and Takahashi, M. (2002). Role of Dok1 in cell signaling mediated by Ret tyrosine kinase. J. Biol. Chem. *277*, 32781–32790.

Pollard, T.D. (2002). Actin and actin-binding proteins. In Cell Biology, T.D. Pollard and W.C. Earnshaw, eds. (New York: W.B. Saunders), pp. 557–577.

Pollard, T.D., and Borisy, G.G. (2003). Cellular motility driven by assembly and disassembly of actin filaments. Cell *112*, 453–465.

Revenu, C., Athman, R., Robine, S., and Louvard, D. (2004). The co-workers of actin filaments: from cell structures to signals. Nat. Rev. Mol. Cell Biol. *5*, 1–12.

Ridley, A.J. (2001). Rho GTPases and cell migration. J. Cell Sci. *114*, 2713–2722.

Ridley, A.J., Schwartz, M.A., Burridge, K., Firtel, R.A., Ginsberg, M.H., Borisy, G., Parsons, J.T., and Horwitz, A.R. (2003). Cell migration: integrating signals from front to back. Science *302*, 1704–1709.

Rivero, F., Koppel, B., Peracino, B., Bozzaro, S., Siegert, F., Weijer, C.J., Schleicher, M., Albrecht, R., and Noegel, A.A. (1996). The role of the cortical cytoskeleton: F-actin crosslinking proteins protect against osmotic stress, ensure cell size, cell shape and motility, and contribute to phagocytosis and development. J. Cell Sci. *109*, 2679–2691.

Roberts, M.S., Woods, A.J., Dale, T.C., van der Sluijs, P., and Norman, J.C. (2004). Protein kinase B/Akt acts via glycogen synthase kinase 3 to regulate recycling of αvβ3 and α5β1 integrins. Mol. Cell. Biol. *24*, 1505–1515.

Scheid, M.P., and Woodgett, J.R. (2001). PKB/AKT: functional insights from genetic models. Nat. Rev. Mol. Cell Biol. *2*, 760–768.

Sechi, A.S., and Wehland, J. (2000). The actin cytoskeleton and plasma membrane connection: PtdIns(4,5)P_2 influences cytoskeletal protein activity at the plasma membrane. J. Cell Sci. *113*, 3685–3695.

Servant, G., Weiner, O.D., Herzmark, P., Balla, T., Sedat, J.W., and Bourne, H.R. (2000). Polarization of chemoattractant receptor signaling during neutrophil chemotaxis. Science *287*, 1037–1040.

Small, J.V., Stradal, T., Vignal, E., and Rottner, K. (2002). The lamellipodium: where motility begins. Trends Cell Biol. *12*, 112–120.

Stossel, T.P., Condeelis, J., Cooley, L., Hartwig, J.H., Noegel, A., Schleicher, M., and Shapiro, S.S. (2001). Filamins as integrators of cell mechanics and signaling. Nat. Rev. Mol. Cell Biol. *2*, 138–145.

Takahashi, M. (2001). The GDNF/RET signaling pathway and human disease. Cytokine Growth Factor Rev. *12*, 361–373.

Usukura, J. (1993). Rapid freezing and subsequent preparation methods in retinal cell biology. In Methods in Neurosciences, P.A. Hargrave, ed. (San Diego: Academic Press, Inc.), pp. 37–53.

Vanhaesebroeck, B., Leevers, S.J., Ahmadi, K., Timms, J., Katso, R., Driscoll, P.C., Woscholski, R., Parker, P.J., and Waterfield, M.D. (2001). Synthesis and functions of 3-phosohorylated inositol lipids. Annu. Rev. Biochem. *70*, 535–602.

Vivanco, I., and Sawyers, C.L. (2002). The phosphatidylinositol 3-kinase-Akt pathway in human cancer. Nat. Rev. Cancer *2*, 489–501.

Watanabe, T., Wang, S., Noritake, J., Sato, K., Fukata, M., Takefuji, M., Nakagawa, M., Izumi, N., Akiyama, T., and Kaibuchi, K. (2004). Interaction of IQGAP1 links APC to Rac1, Cdc42, and actin filaments during cell polarization and migration. Dev. Cell *7*, 871–883.

Yoshimura, T., Kawano, Y., Arimura, N., Kawabata, S., Kikuchi, A., and Kaibuchi, K. (2005). GSK-3β regulates phosphorylation of CRMP-2 and neuronal polarity. Cell *120*, 137–149.

Zhou, G., Zhuo, Y., King, C.C., Fryer, B.H., Bokoch, G.M., and Field, J. (2003). Akt phosphorylation of serine 21 on Pak1 modulates Nck binding and cell migration. Mol. Cell. Biol. *23*, 8058–8069.

Accession Numbers

The human Girdin cDNA sequence has been deposited in GenBank/EMBL/DDBJ with the accession number AB201172.

PNAS
Proceedings of the National Academy of Sciences of the United States of America www.pnas.org

L-citrulline and L-arginine supplementation retards the progression of high-cholesterol-diet-induced atherosclerosis in rabbits

Toshio Hayashi, Packiasamy A. R. Juliet, Hisako Matsui-Hirai, Asaka Miyazaki, Akiko Fukatsu, Jun Funami, Akihisa Iguchi, and Louis J. Ignarro

PNAS 2005;102;13681-13686; originally published online Sep 12, 2005;
doi:10.1073/pnas.0506595102

L-citrulline and L-arginine supplementation retards the progression of high-cholesterol-diet-induced atherosclerosis in rabbits

Toshio Hayashi*†, Packiasamy A. R. Juliet*, Hisako Matsui-Hirai*, Asaka Miyazaki*, Akiko Fukatsu*, Jun Funami*, Akihisa Iguchi*, and Louis J. Ignarro†‡§

*Department of Geriatrics, Nagoya University Graduate School of Medicine, 65 Tsuruma-cho, Showa-ku, Nagoya 466-8550, Japan; and ‡Department of Molecular and Medical Pharmacology, David Geffen School of Medicine, University of California, 650 Charles E. Young Drive South, Los Angeles, CA 90095

Contributed by Louis J. Ignarro, August 6, 2005

The objective of this study was to evaluate the influence of ingested L-arginine, L-citrulline, and antioxidants (vitamins C and E) on the progression of atherosclerosis in rabbits fed a high-cholesterol diet. The fatty diet caused a marked impairment of endothelium-dependent vasorelaxation in isolated thoracic aorta and blood flow in rabbit ear artery *in vivo*, the development of atheromatous lesions and increased superoxide anion production in thoracic aorta, and increased oxidation-sensitive gene expression [Elk-1 and phosphorylated cAMP response element-binding protein]. Rabbits were treated orally for 12 weeks with L-arginine, L-citrulline, and/or antioxidants. L-arginine plus L-citrulline, either alone or in combination with antioxidants, caused a marked improvement in endothelium-dependent vasorelaxation and blood flow, dramatic regression in atheromatous lesions, and decrease in superoxide production and oxidation-sensitive gene expression. These therapeutic effects were associated with concomitant increases in aortic endothelial NO synthase expression and plasma NO_2^- + NO_3^- and cGMP levels. These observations indicate that ingestion of certain NO-boosting substances, including L-arginine, L-citrulline, and antioxidants, can abrogate the state of oxidative stress and reverse the progression of atherosclerosis. This approach may have clinical utility in the treatment of atherosclerosis in humans.

antioxidant | nitric oxide | amino acids | endothelial nitric oxide synthase

Atherosclerosis is an inflammatory disease (1) characterized by vascular endothelial cell dysfunction and diminished production of NO (2–5). Endothelial NO synthase (eNOS) gene transfer can reduce atherogenesis in hypercholesterolemic animals (6). NO is a widespread signaling molecule in the cardiovascular system, which functions in multiple ways to protect against the initiation and progression of atherosclerosis (7–9). For example, NO aids in preventing the adhesion and aggregation of blood cells and platelets along the endothelial cell lining in blood vessels (7, 8) and is a potent inhibitor of vascular smooth muscle cell proliferation (10). NO is a potent antioxidant that can elicit antiinflammatory effects by scavenging certain reactive oxygen species (11–13), and it can prevent the oxidation of low-density lipoprotein cholesterol and thereby retard the progression of atherosclerosis (5, 14). Moreover, NO deficiency is generally associated with up-regulation of oxidation-sensitive genes, whereas increased NO production leads to decreased expression of oxidation-sensitive genes (7, 15). NO is synthesized by NOS, which utilizes L-arginine as substrate and produces L-citrulline as the second reaction product. L-arginine can be synthesized from L-citrulline in endothelial and other cell types, thereby providing a recycling pathway for the conversion of L-citrulline to NO via L-arginine (16–19).

The oral administration of L-arginine to animals (7, 12, 20–26) and humans (5, 8, 27–29) has been demonstrated to slow the progression of atherosclerosis or its component processes. Likewise, antioxidants can elicit antiatherosclerotic effects (13, 30–33). Coadministration of antioxidants with L-arginine produced an enhanced antiatherosclerotic response (7, 13). The mechanism of action of L-arginine appears to be increased production of NO, whereas antioxidants likely work by protecting the newly formed NO against destruction by reactive oxygen species. The principal explanation for the therapeutic response to L-arginine has been increased substrate availability to eNOS, for example by competing with asymmetric dimethylarginine, an endogenous competitive inhibitor of eNOS that is prevalent in states of atherosclerosis (33–36). In two recent studies, however, chronic administration of L-arginine to low-density lipoprotein receptor-deficient mice produced a marked increase in expression of eNOS protein (25, 26). Thus, up-regulation of eNOS could explain the antiatherosclerotic response to L-arginine. The oral administration of L-citrulline, as a precursor to L-arginine and NO, was reported to be beneficial in sickle cell disease in humans (37). Studies indicate that the L-citrulline to L-arginine recycling pathway in endothelial cells may be the principal mechanism for sustaining localized L-arginine availability for eNOS-catalyzed NO production (17–19). The objective of the present study was to examine the actions of L-arginine, L-citrulline, and antioxidants administered orally to rabbits with atherosclerosis.

Materials and Methods

Animals, Protocols, and Metabolic Treatments. A total of 49 New Zealand White male rabbits, aged 3–4 months and weighing 2.0 to 2.4 kg, were housed individually at 20 ± 3°C with free access to water. Rabbits were divided into the following seven groups (six rabbits per group), depending on diet; amino acid, vitamin, and test agents were administered for 12 weeks: Gp1-HCD, high-cholesterol diet (HCD) (standard diet plus 0.5% cholesterol); Gp2-Arg, HCD plus L-arginine (2.5% in drinking water); Gp3-Cit, HCD plus L-citrulline (2.0% in drinking water); Gp4-Arg+Cit, HCD plus L-arginine and L-citrulline; Gp5-Vit, HCD plus vitamin C (sodium ascorbate; 0.25% in drinking water) and vitamin E (DL-α-tocopherol; 150 mg/kg per day by oral gavage); Gp6-Arg+Vit, HCD plus L-arginine and vitamins C and E; and Gp7-Mix, HCD plus L-arginine, L-citrulline and vitamins C and E. In some experiments, an additional group was studied, Gp8-C (control; standard diet; $n = 6$). Feeding was restricted per rabbit to 120 g per day. Blood was sampled 24 h after the last feeding.

Abbreviations: NO_X, NO_2^- + NO_3^-; eNOS, endothelial NO synthase; *p*-CREB, phosphorylated cAMP response element-binding protein; HCD, high-cholesterol diet; Gp*n*, group *n*.

†To whom correspondence may be addressed. E-mail: hayashi@med.nagoya-u.ac.jp or lignarro@mednet.ucla.edu.

§L.J.I. wishes to disclose that he helped develop and has a financial interest in a commercially available dietary supplement that contains some of the amino acids and antioxidants studied in this report.

Table 1. Plasma levels of lipid, NO products, and cGMP

	Gp1-HCD	Gp2-Arg	Gp3-Cit	Gp4-Arg + Cit	Gp5-Vit	Gp6-Vit + Arg	Gp7-Mix
T.Chol., mg/dl	1,758 ± 162	1,584 ± 104	1,460 ± 210	1,350 ± 178	1,473 ± 171	1,662 ± 162	1,257 ± 172
Triglycerides, mg/dl	104.2 ± 7.1	120.7 ± 10.5	89.8 ± 4.4	88.8 ± 4.5	98.4 ± 7.1	120.5 ± 8.3	72.3 ± 6.9
HDL-C, mg/dl	29.1 ± 4.8	29.4 ± 3.3	26.0 ± 3.2	34.4 ± 4.1	33.5 ± 5.3	33.9 ± 4.5	35.8 ± 4.1
$NO_2^- + NO_3^-$, nM	25.1 ± 2.6	27.3 ± 4.1	25.2 ± 4.0	35.1 ± 5.2*	17.2 ± 3.6	26.8 ± 1.8	29.1 ± 2.1*
cGMP, pg/ml	19.1 ± 3.3	18.9 ± 2.8	32.3 ± 3.7	36.7 ± 5.2*	19.3 ± 4.5	32.9 ± 6.3	41.0 ± 6.1*
Body weight, kg	3.12 ± 0.31	2.96 ± 0.40	3.11 ± 0.31	3.02 ± 0.21	3.23 ± 0.34	2.97 ± 0.23	3.02 ± 0.32

Refer to *Materials and Methods* for the definitions of the treatment groups. Data are expressed as the mean ± SEM from six rabbits per group. T. Chol, total cholesterol; HDL-C, high-density lipoprotein-cholesterol.
*Significant difference ($P < 0.05$) vs. Gpl-HCD.

All experiments were conducted in accordance with the institutional guidelines for animal research.

Determination of Plasma Lipids, NO Metabolites, and cGMP. Total cholesterol and triglyceride levels were measured as described (38). HDL–cholesterol was determined after precipitation with phosphotungstate–$MgCl_2$ (39). Plasma NO_2^- plus NO_3^- (NO_X) was measured by using an NO detector–HPLC system (ENO10; Eicom, Kyoto, Japan), as described (40). Plasma cGMP concentration was determined by specific RIA (RPN226, Amersham Pharmacia) (41).

Isometric Tension Measurements. After 12 weeks of treatment, rabbits were killed by exsanguination after anesthesia with pentobarbital (50 mg/kg i.v.). The thoracic aorta was excised from the orifice of the left first costal artery down to the diaphragm, cleaned, and sliced into 2-mm-wide transverse rings. Aortic rings were mounted in organ chambers, and isometric tension was measured exactly as described (6). Rings were contracted submaximally with prostaglandin $F_{2\alpha}$, and endothelium-dependent relaxation elicited by acetylcholine chloride and endothelium-independent relaxation by nitroglycerin (Nihon Kayaku, Tokyo) was determined. In some experiments, indomethacin (5×10^{-6} M) was added 60 min before the experiment to rule out any influence of prostanoids on smooth muscle tone. All indicated concentrations are final concentrations in the bath medium.

Tissue Blood Flow Determined by Laser Doppler Perfusion Imaging. To investigate blood flow near the right central ear artery, we used a laser Doppler imaging system (laser Doppler perfusion imager PIMII, Perimed AB, Linköping, Sweden), as described (42, 43). This method provides a 2D mapping of blood flow in tissues and is based on the principles of laser Doppler flowmetry (42).

Histological Evaluation of Atherosclerosis in Rabbit Aorta. Cross sections of the thoracic aorta used for the evaluation of endothelium-dependent relaxation were stained with van Gieson's elastic stain to determine intimal thickness. Morphometric analysis was performed as described by Weiner *et al.* (44) and modified by this laboratory (6). Six samples from each rabbit aorta were analyzed.

Detection of Superoxide Anion ($O_2^{\bullet-}$) in Rabbit Aorta. $O_2^{\bullet-}$ in each aortic segment was assayed by measuring the intensity of chemiluminescent probes in the presence of a Cypridina luciferin analog, 2-methyl-6-(*p*-methoxyphenyl)-3,7-dihydroimidazol, 2-apyrazine-3-one (45). Briefly, the generation of $O_2^{\bullet-}$ from a 2-mm length of aorta was detected by using a luminescence reader (BLR-201, Aloka, Tokyo), in the absence and presence of superoxide dismutase to verify specificity of the assay for $O_2^{\bullet-}$.

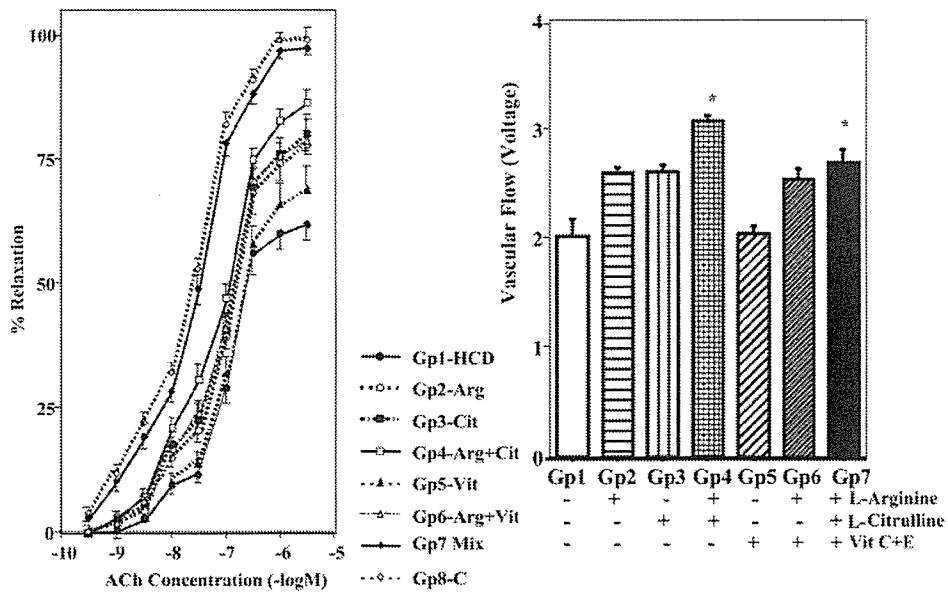

Fig. 1. Vascular responses of thoracic aortas of rabbits. (*Left*) Cumulative concentration-response curves to acetylcholine (ACh) during contraction evoked by prostaglandin $F_{2\alpha}$ (2.6×10^{-6} M) in thoracic aortas from eight groups of rabbits ($n = 6$ per group). (*Right*) Rate of blood flow near the right central ear artery in seven groups of rabbits ($n = 6$ per group). Refer to *Materials and Methods* for definitions of treatment groups. Data are illustrated as the mean ± SEM from six rabbits per group. *, Significant difference ($P < 0.05$) vs. Gp1-HCD.